

University of New Hampshire

University of New Hampshire Scholars' Repository

Doctoral Dissertations

Student Scholarship

Winter 1975

A MATHEMATICAL MODEL OF INTERPLANETARY RADIO SCINTILLATION, IN THE WEAK-SCATTERING REGIME

DONALD GRANT MITCHELL

Follow this and additional works at: <https://scholars.unh.edu/dissertation>

Recommended Citation

MITCHELL, DONALD GRANT, "A MATHEMATICAL MODEL OF INTERPLANETARY RADIO SCINTILLATION, IN THE WEAK-SCATTERING REGIME" (1975). *Doctoral Dissertations*. 1107.
<https://scholars.unh.edu/dissertation/1107>

This Dissertation is brought to you for free and open access by the Student Scholarship at University of New Hampshire Scholars' Repository. It has been accepted for inclusion in Doctoral Dissertations by an authorized administrator of University of New Hampshire Scholars' Repository. For more information, please contact Scholarly.Communication@unh.edu.

INFORMATION TO USERS

This material was produced from a microfilm copy of the original document. While the most advanced technological means to photograph and reproduce this document have been used, the quality is heavily dependent upon the quality of the original submitted.

The following explanation of techniques is provided to help you understand markings or patterns which may appear on this reproduction.

- 1. The sign or "target" for pages apparently lacking from the document photographed is "Missing Page(s)". If it was possible to obtain the missing page(s) or section, they are spliced into the film along with adjacent pages. This may have necessitated cutting thru an image and duplicating adjacent pages to insure you complete continuity.**
- 2. When an image on the film is obliterated with a large round black mark, it is an indication that the photographer suspected that the copy may have moved during exposure and thus cause a blurred image. You will find a good image of the page in the adjacent frame.**
- 3. When a map, drawing or chart, etc., was part of the material being photographed the photographer followed a definite method in "sectioning" the material. It is customary to begin photoing at the upper left hand corner of a large sheet and to continue photoing from left to right in equal sections with a small overlap. If necessary, sectioning is continued again — beginning below the first row and continuing on until complete.**
- 4. The majority of users indicate that the textual content is of greatest value, however, a somewhat higher quality reproduction could be made from "photographs" if essential to the understanding of the dissertation. Silver prints of "photographs" may be ordered at additional charge by writing the Order Department, giving the catalog number, title, author and specific pages you wish reproduced.**
- 5. PLEASE NOTE: Some pages may have indistinct print. Filmed as received.**

Xerox University Microfilms

300 North Zeeb Road
Ann Arbor, Michigan 48106

76-11,683

MITCHELL, Donald Grant, 1949-
A MATHEMATICAL MODEL OF INTERPLANETARY
RADIO SCINTILLATION, IN THE WEAK-SCATTERING
REGIME.

University of New Hampshire, Ph.D., 1975
Physics, astronomy and astrophysics

Xerox University Microfilms, Ann Arbor, Michigan 48106

A MATHEMATICAL MODEL OF INTERPLANETARY RADIO
SCINTILLATION, IN THE WEAK-SCATTERING REGIME

by

DONALD G. MITCHELL

B.A., Univ. of Michigan, 1971

A THESIS

Submitted to the University of New Hampshire

In Partial Fulfillment of

The Requirements for the Degree of

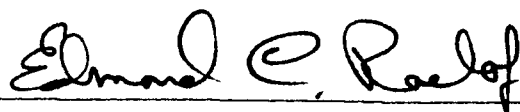
Doctor of Philosophy

Graduate School

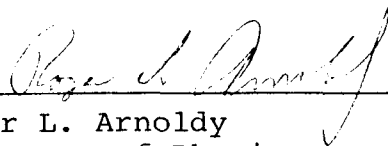
Department of Physics

December, 1975

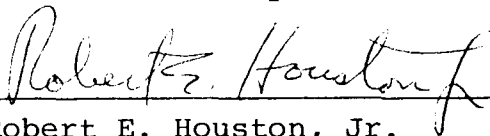
This thesis has been examined and approved.



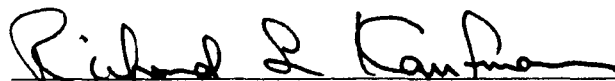
Thesis director, Edmond C. Roelof
Senior Scientist, Johns Hopkins University
Applied Physics Laboratory



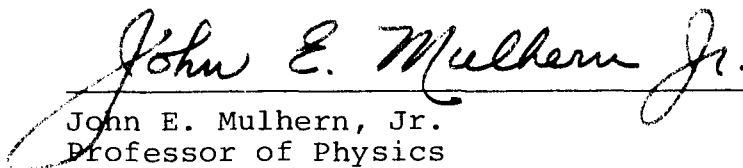
Roger L. Arnoldy
Professor of Physics



Robert E. Houston, Jr.
Professor of Physics



Richard L. Kaufmann
Professor of Physics



John E. Mulhern, Jr.
Professor of Physics

November 25, 1975

Date

ACKNOWLEDGEMENTS

I would like to express my deep gratitude and appreciation for the time, effort, support, and enthusiasm contributed over the course of this work by Dr. E.C. Roelof, my thesis advisor. I would like to acknowledge gratefully the many useful and rewarding discussions and exchanges with Dr. Willard Cronyn. I would also like to thank Susan Horner for a fast and professional typing job when I most needed it.

This work was supported by grants from the University of Iowa and the Johns Hopkins University Applied Physics Laboratory.

TABLE OF CONTENTS

LIST OF TABLES and LIST OF ILLUSTRATIONS.	v
ABSTRACT.	viii
I. INTRODUCTION.	1
II. THEORY.	5
A. General	5
B. For Power Law Spectrum.	17
III. NUMERICAL TECHNIQUE	21
A. Expansion of J Function	21
B. Integration over Extended Medium.	29
C. Scintillation Index and Scale	30
D. Scattering Power Profile.	31
IV. DISCUSSION.	38
A. Thin Slab Spectrum.	38
B. Extended Medium Spectrum and Moments.	39
C. Effects of Band-Passing Data.	40
D. Fits to Data.	41
V. SUMMARY	48
BIBLIOGRAPHY.	50
APPENDIX A.	54
APPENDIX B.	57
APPENDIX C.	61

LIST OF TABLES

1. Parameters of the COCOA-CROSS RADIO TELESCOPE. 67

LIST OF ILLUSTRATIONS

1. Geometry of the thin slab scattering, showing the orientation of variables used in the text. 6
- 2a. Contours of the asymptotic expansion of the real part of the confluent hypergeometric function $U(\frac{1}{2}, \frac{3-q}{2}, \xi + i\eta)$ in the logarithmically spaced $\xi - \eta$ complex plane. 22
- 2b. Same as 2a, for the imaginary part of U. 23
- 3a. Error plot of J function in the $\log(2S)$ vs $\log(4S_1)$ plane, for power law index (q) equal to 4. S is proportional to the frequency of the intensity fluctuation squared (ν^2), and S_1 is proportional to the frequency corresponding to the source angular size, squared. 24
- 3b. Same as 3a, with q equal to 3.6 25
- 3c. Same as 3a, with q equal to 3.2 26
4. Thin slab, point source theoretical spectrum shown on an arbitrary log-log scale. Points of note are the Fresnel turn over to a flattening of lower frequencies, and the Fresnel ripple imposed on the power law at higher frequencies. 27

5.	Scintillation index vs elongation angle (ϵ) for band-passed and complete spectra, at several source sizes (Ω)	32
6.	Second moment vs elongation angle for band-passed and complete spectra, for several source sizes.	33
7a.	Computed extended medium spectra (heavy line), computed using five different slabs through the quiet medium, for q equal to 4.0. Also shown are the separate spectra for each slab, indicating the relative strength of the scattering at a given frequency for a particular slab. The source size is $\Omega = .1''$, the elongation angle 60°	34
7b.	Same as 7a, with $\Omega = .5''$	35
8.	Relative contribution to the total scattered intensity from different distances (L 's) along the earth-source line, for different elongation angles (ϵ). Source size is $.1''$	37
9a.	Fit to spectrum published by Lovelace et al., 1970. A quiet medium is assumed, and several source sizes are shown. Power law index (q) equals 3.6	42
9b.	Same as 9a, but with q equal to 3.2, and with different source sizes.	43
10a.	Fit to spectrum of radio source 3C216 taken with COCOA-CROSS antenna. Proper fit lies between the two source sizes used. Note that the computed spectra are off set vertically for clarity. The data were corrected for noise background.	45

10b.	Fit to spectrum of 3C144 taken with COCOA-CROSS antenna. Same day as the spectrum of 10a; the same velocity and power law slope were fit as in 10a but a slightly smaller source size.	46
C 1	Block Diagram of COCOA CROSS Radio Telescope.	69
C 2	Observations on COCOA CROSS Telescope, October 5, 1974	70
C 3	Observations on COCOA CROSS Telescope between November 24 and November 27, 1974	71

ABSTRACT

A MATHEMATICAL MODEL OF INTERPLANETARY RADIO SCINTILLATION IN THE WEAK SCATTERING REGIME

by

DONALD G. MITCHELL

Interplanetary scintillations are modeled under the assumption of a power-law electron density fluctuation power spectrum. The model provides the means for quickly interpreting large quantities of data, even on a real time basis. This is important for two reasons. First, interpretation on a real time basis is essential to the ultimate goal of predicting the arrival at earth of interplanetary disturbances days before their arrival. Second, fast (and inexpensive) interpretation is needed in order to process diurnal observation on up to 200 sources continuously for a year or more. This large amount of data is needed both to track disturbances in the solar wind, and to observe spatial- and long-range temporal electron density fluctuation profiles in the interplanetary medium.

The modeling is accomplished through several steps. An analytic expression is found for the integral expression for the weak-scattering power spectrum from a thin slab of the medium. This expression is then approximated for the sake of tractability, with a maximum error of ten percent. The thin slab result is then integrated numerically through the medium

along the line of sight to a radio source, thus building up the extended medium spectrum. Further results include the zeroth and second moments of the spectrum, as functions of sun-earth-source angle (elongation angle) for a quiet interplanetary medium.

Fits to published and unpublished data are presented, which indicate a power-law index of 3.2 - 3.6, and are interpreted in terms of solar wind velocity and density profile, as well as source angular scale.

CHAPTER I

INTRODUCTION

Radio scintillation observations of the solar wind have been analyzed for a decade, with several models emerging for the power spectrum of the electron density irregularities.

The two basic models are a Gaussian and a power-law wave-number dependence for the electron density power spectrum. This paper will concentrate on the power-law model. A power law was first suggested in 1970 by a number of authors: Cronyn (1970); Hollweg (1970); Jokipii (1970); Jokipii and Hollweg (1970); and Lovelace et al. (1970). These authors argued for a power-law dependence on the basis of an increasing realization that not only could the data be fit with a power law, but also because the directly measurable spectra of the other solar wind parameters were found to exhibit power-law dependence. Cronyn (1972) presented evidence that in fact the spectrum measured by radio scintillation was consistent with the power law measured at much lower wave numbers by satellites.

The functional form of the power law has several variations: an exact isotropic power law (k^{-q}), suggested by Jokipii (1970), Jokipii and Hollweg (1970), Lovelace (1970), and Young (1971); a form including parameters for elongation of the irregularities $(\gamma k_x^2 + \epsilon k_y^2 + k_z^2)^{-q/2}$, suggested by Cronyn (1970, 1972), Lovelace (1970) and Rufenach (1972); a

parameter for an outer scale to limit the power at low wave numbers $(k_0^2 + k^2)^{-q/2}$, Cronyn (1970), Matheson and Little (1971), Callahan (1974); and a form with a parameter for an inner scale $(k_0^2 + k^2)^{-q/2} \exp(-k^2/2k_i^2)$. This last form was suggested (not always in this strict functional form) by Hollweg (1970), Jokipii and Hollweg (1970), Matheson and Little (1971), Rickett (1973).

In this dissertation, we calculate analytic expressions for the thin-screen frequency power spectrum for the scintillations detected at a radio telescope. We use a power law with free parameters for radio source angular scale and axial ratio, slope at large wave numbers, and elongation of electron density irregularities along the direction of the solar wind velocity. Much of the discussion of these parameters has been covered by other authors, perhaps most completely and concisely (although semi-quantitatively) by Matheson and Little (1971). However, to our knowledge this is the first time many of the observable functions have been expressed analytically. In some cases, these expressions will facilitate quick comparison with actual data. They are extended to include the thick-screen model of Young (1971), which, by integrating the thin-screen contributions over many screens, builds up the weak-scattering, thick-screen scintillation spectrum. We demonstrate here that the main contribution to the extended medium comes from different regions of the medium along the line of sight at different frequencies.

In addition to the model spectra, the zeroth and second moments of the spectra are also obtained. The zeroth moment is known as the scintillation index, while the second moment is often referred to as the frequency "scale". Both of these moments are experimentally more easily obtainable than the spectrum itself, and so are included in this work. They are particularly useful in investigating long term and spatial effects.

Instrument and radio-source parameter effects must also be considered. Instrument effects have already been dealt with satisfactorily by other authors (e.g. Readhead, 1971, Budden and Uscinski, 1972) and will not be dealt with here. In most cases these effects are negligible.

Source parameters affect the system response drastically, however. The most obvious manifestation of source effects is the observation that not all sources produce measurable scintillation. The parameter responsible for this effect is the source angular diameter. Large angular diameter sources do not scintillate. The reason for this might best be illustrated with the analogous phenomenon of atmospheric refraction of starlight, producing optical scintillation, or twinkling. Neither the planets nor the moon nor the sun exhibit this twinkling, as their angular diameters are greater than those of the refracting irregularities, and so the diffraction pattern is "smeared out". One sees the sum of the patterns produced by each point on the disc of the source, and that sum is over many random uncorrelated patterns, and so does not change statistically.

Another source effect which is less obvious is that associated with the axial ratio of an (idealized) elliptical source. This effect changes the point in the observed frequency spectrum at which the angular diameter effects become dominant, and it is a function of the angle between the (projected) solar wind velocity vector and the major axis of the source. By modeling the medium and sources using these parameters, it is then possible to predict the response of a radio telescope to various conditions in the solar wind and also to gain information on new radio sources.

The immediate purpose of this investigation is to be able to quickly reduce raw data to discover the location and the strength of disturbances propagating through the interplanetary medium, and predict on a real-time basis when these disturbances will intercept the earth or spacecraft. In order to treat this subject thoroughly, a brief review of the theory of radio scintillation follows.

CHAPTER II

THEORY

A. General

In examining radio wave scattering in the interplanetary medium, approximations based on the physics of the scattering must be made in order to treat the subject mathematically. First, we have in the interplanetary medium a tenuous plasma whose conductivity can be written $\sigma \approx iN_e e^2/m\omega$ where N_e is the electron density (ions are ignored, due to their large inertial mass), and e is the charge on an electron. The electron mass is m , and ω is the frequency of the propagating wave in the medium (static fields can't exist for long periods over distances greater than a Debye length). There is essentially no damping due to collisions, and the purely imaginary conductivity means there are no resistive losses (the current and electric field are out of phase). The effect of the interplanetary magnetic field on the dispersion relation of waves of the frequencies considered here is completely negligible (one part in 10^6). The dispersion relation can then be written

$$(1) \quad k^2 = \frac{\omega^2}{c^2} \left(1 - \frac{\omega_p^2}{\omega^2} \right)$$

where

$$(2) \quad \omega_p^2 = 4\pi N_e e^2/m_e$$

where ω_p is the plasma frequency. Writing k equal to $n\omega/c$

where n is the index of refraction, we have

$$(3) \quad n^2 \approx \left(1 - \omega_p^2/\omega^2 \right)$$

which is valid in the range ω much greater than ω_p . (This is

certainly the case here, as ω is greater than or equal to

10^8 sec^{-1} , while for the interplanetary medium, ω_p is about 10^5 sec^{-1} .) The index of refraction is a function of the electron

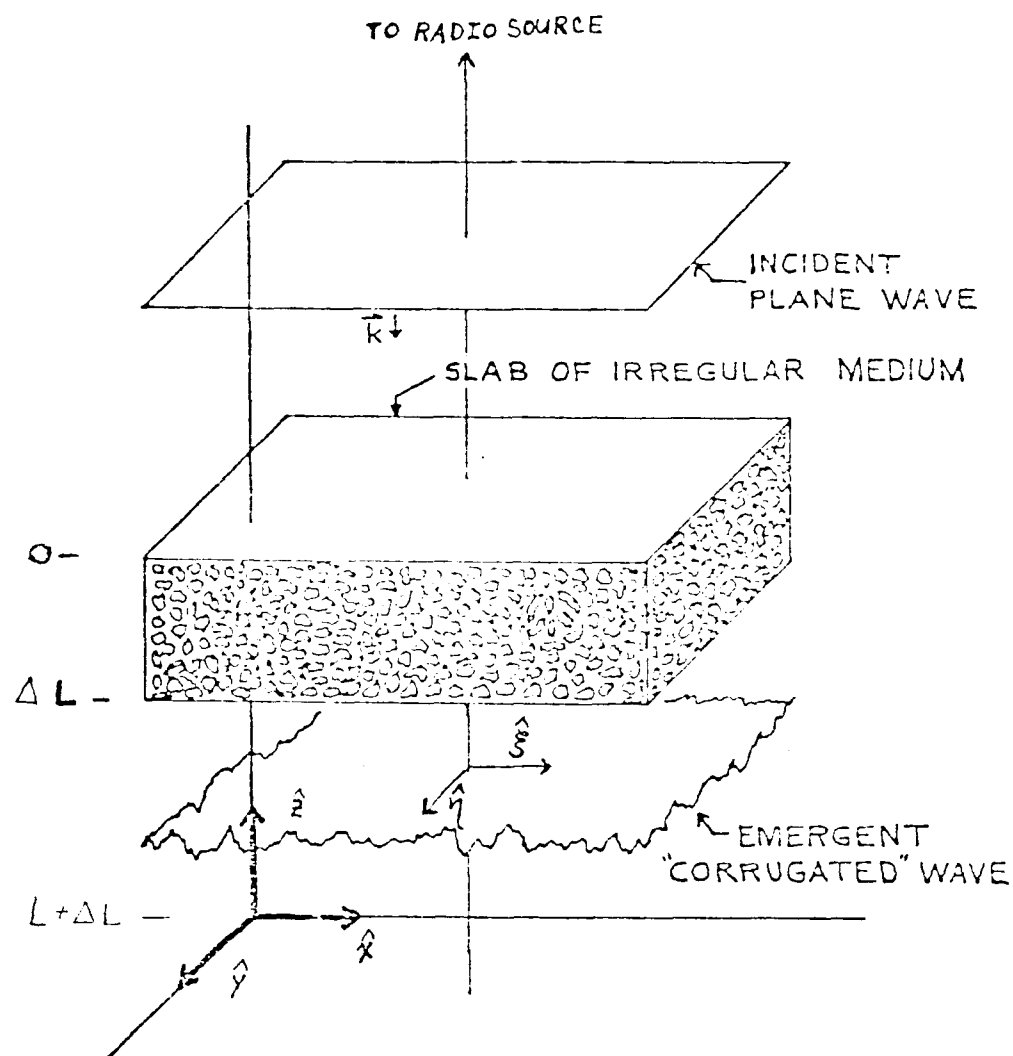


FIGURE 1

SPATIAL APPEARANCE OF SURFACE OF CONSTANT PHASE BEFORE AND AFTER SCATTERING. Spatial fluctuation Δz in surface of constant phase of emergent wave corresponds to phase fluctuation $2\pi\Delta z/\lambda$.

Adapted from Figure by Cronyn, 1970.

density so that spatial variations of N_e produce spatial variations in n .

The geometry shown in Figure 1 will be referred to in the subsequent discussion. The problem will be idealized to a plane wave traveling along the z axis, which passes through a slab of a medium with random irregularities in index of refraction, and leaves the slab with a random spatial phase perturbation on the original plane wave. The wave is still moving in the z direction, essentially.

The calculation of the phase perturbation is done using the eikonal approximation of geometrical optics. This is a good approximation because (1) the variations in index of refraction are small, and (2) the wavelength of the incident plane wave is much smaller than the typical scale size of the irregularities. In this case, λ is in the range .1 - 10m, and L , the scale size is typically on the order of 10^2 km. This approximation allows us to write

$$(4) \quad \psi = \psi_0 e^{ik_0(nz - ct)}$$

(See Born and Wolf, 1965, page 110 for discussion) where k_0 is the wave number of the radiation in free space and n is the index of refraction. The letter ψ_0 is a scalar quantity representing the amplitude of either the \vec{E} or \vec{B} field in the propagating wave; n is a function of z , ξ , and η where ξ and η are coordinates in the plane perpendicular to the z axis. Thus the total spatial phase change of the wave from entry to exit from the slab is

$$(5) \quad \int_0^{\Delta L} k_0 n(\xi, \eta, z) dz$$

Now writing

$$(6) \quad \begin{aligned} n &= \bar{n} + (n - \bar{n}) \\ &= \bar{n} + \delta n(\xi, \eta, z) \end{aligned}$$

where \bar{n} is the average index of refraction in the slab and δn is the random fluctuation, the phase change becomes

$$(7) \quad k_0 \bar{n} \Delta L + k_0 \int_0^{\Delta L} \delta n(\xi, \eta, z) dz$$

The term $k_0 \bar{n} \Delta L$ is not of interest, as it is a constant phase shift and does not cause diffraction. The second term, however, varies at different points along the wave front and creates a random phase shift as a function of ξ and η . Let us set

$$(8) \quad \phi(\xi, \eta) \equiv k_0 \int_0^{\Delta L} \delta n(\xi, \eta, z) dz$$

So aside from the constant phase shift $k_0 \bar{n} \Delta L$, which can be ignored

$$(9) \quad \psi_{\Delta L} = \psi_0 e^{ik_0(z-ct)} e^{i\phi(\xi, \eta)}$$

We now introduce the Kirchoff integral from Jackson, 9.5 (1962). This expression yields the resultant wave function (at any point in space) of the transmitted portion of a wave incident on a diffracting screen. It is based on the ideas of superposition of elemental wavelets due to Huygens, and is derived using a Green's function technique. See Jackson for a complete discussion.

$$(10) \quad \psi(\vec{X}) = \frac{1}{4\pi} \oint_S da' \frac{e^{ik_0 R'}}{R'} \left[\nabla' \cdot \vec{\psi} + ik \left(1 + \frac{i}{kR'}\right) \hat{R}' \cdot \vec{\psi}' \right] \cdot \hat{n}$$

where R' is $|\vec{X} - \vec{X}'|$ and in our case S is a surface formed by the exit plane of the slab and a surface at infinity. The time variation is assumed to be $e^{i\omega t}$ and \hat{n} is the outward normal to S . Primed coordinates are in the exit plane of the slab; unprimed are in the observer's plane, i.e. $|\vec{X}'|$ is equal to $\sqrt{\xi^2 + \eta^2 + \Delta L^2}$. If we let the distance from the exit plane to

the observer be L , then $|\vec{X} - \vec{X}'|$ is $[L^2 + (\vec{X} - \vec{X}')^2]^{1/2}$ where $|\vec{X}|$ equals $(x^2 + y^2)^{1/2}$ and $(\vec{X} - \vec{X}')^2$ equals $(x - \xi)^2 + (y - \eta)^2$. If we set both x and y equal to 0, then $|\vec{X} - \vec{X}'|$ is $(L^2 + \xi^2 + \eta^2)^{1/2}$. But as the angular scattering is very small (eikonal approximation), L is much greater than $(\xi^2 + \eta^2)^{1/2}$ so

$$(11) \quad |\vec{X} - \vec{X}'| \sim L + \frac{1}{2L} (\xi^2 + \eta^2).$$

Using this, and noting that

$$\hat{n} \cdot \nabla' = \frac{\partial}{\partial L'}$$

one finds

$$(12) \quad \psi_{\text{observer}} \simeq \frac{ik_0}{2\pi L} e^{ik_0 L} \int d\xi \int d\eta e^{-\frac{ik_0}{2L}(\xi^2 + \eta^2)} e^{i\phi(\xi, \eta)}$$

(assuming the incident ψ_0 had unit amplitude). The slab of medium is moving in the \hat{x} direction at the solar wind velocity.

Thus ϕ is $\phi(\xi - Vt, \eta)$ to the stationary observer, and so

ψ_{observer} is a function of t , also. But we are interested in intensity, $I(t)$, rather than amplitude.

$$(13) \quad I(t) = \psi(t) \psi^*(t)$$

Staying for the time being in the spatial domain, we have

$$(14) \quad I_L(\vec{x}) = \psi_L(\vec{x}) \psi_L^*(\vec{x})$$

where \vec{x} is an implicit function of time. Then

$$(15) \quad I_L(\vec{x}) = \left(\frac{k_0}{2\pi L}\right)^2 \int da_1 \int da_2 e^{i[(k_0/2L)(\vec{x} - \vec{x}_1)^2 - \phi(\vec{x}_1)]} e^{i[(k_0/2L)(\vec{x} - \vec{x}_2)^2 - \phi(\vec{x}_2)]}$$

where $I_L(\vec{x})$ is the intensity seen by the observer as a function of \vec{x} , a two-dimensional vector in the plane \perp to z . The variables \vec{x}_1 and \vec{x}_2 , da_1 and da_2 are vectors and area elements in the exit plane of the slab.

The variation of $I_L(\vec{x})$ with \vec{x} can be expressed in terms of the intensity auto-correlation function, or in terms of the Fourier transform of the auto-correlation function, the intensity power spectrum. The auto-correlation function is defined

$$(16) \quad m^2 \rho_I(\vec{r}) = \left\langle [I_L(\vec{x}) - 1] [I_L(\vec{x} + \vec{r}) - 1] \right\rangle$$

$$(17) \quad = \left\langle I_L(\vec{x}) I_L(\vec{x} + \vec{r}) \right\rangle - \left\langle I_L(\vec{x}) \right\rangle - \left\langle I_L(\vec{x} + \vec{r}) \right\rangle + 1$$

but, as $I_L(\vec{x})$ is normalized to one, and a conserved quantity, the ensemble average $\langle I_L(\vec{x}) \rangle$ equals unity. So

$$(18) \quad m^2 \rho_I(\vec{r}) = \left\langle I_L(\vec{x}) I_L(\vec{x} + \vec{r}) \right\rangle - 1$$

where m is the scintillation index, which is the R.M.S. variation in the observed intensity, normalized to unity. Rearranging this expression and substituting the integral expressions for $I_L(\vec{x})$, and transforming coordinates ($\vec{x} - \vec{x}_1$) goes to \vec{x}_1 and likewise, for \vec{x}_2 , \vec{x}_3 and \vec{x}_4), we have

$$(19) \quad m^2 \rho_I(\vec{r}) + 1 = \left(\frac{k_0}{2\pi L} \right)^4 \int da_1 da_2 da_3 da_4 \left[e^{-\frac{i k_0}{2L} (\vec{x}_1^2 - \vec{x}_2^2 + \vec{x}_3^2 - \vec{x}_4^2)} \cdot \left\langle e^{i(\phi_1 - \phi_2 + \phi_3 - \phi_4)} \right\rangle \right]$$

where

$$(20) \quad \phi_1 = \phi(\vec{x} + \vec{x}_1), \quad \phi_2 = \phi(\vec{x} + \vec{x}_2), \quad \phi_3 = \phi(\vec{x} + \vec{x}_3 + \vec{r}),$$

and

$$(21) \quad \phi_4 = \phi(\vec{x} + \vec{x}_4 + \vec{r})$$

Now the ensemble averaging applies only to the random-phase exponential, as that is the only quantity which is a function of \vec{x} .

As δN_e , and therefore ϕ , is Gaussian distributed and has a zero mean, we can use Gaussian statistics on it. Following Mercier (1962) we will use the following mathematical relations:

$$(22) \quad \int_{-\infty}^{\infty} d\chi_1 \int_{-\infty}^{\infty} d\chi_2 \frac{k}{2\pi\epsilon} g(\chi_1 - \chi_2) e^{\frac{i k}{2\epsilon} (\chi_1^2 - \chi_2^2)} = g(0)$$

where g is any well behaved function, and

$$(23) \quad \langle \exp(i\psi) \rangle = \exp(-\frac{1}{2} \langle \psi^2 \rangle)$$

where ψ is any sum of real Gaussian variables. Then

$$(24) \quad \langle e^{i(\phi_1 - \phi_2 + \phi_3 - \phi_4)} \rangle = e^{-\frac{1}{2} \langle \phi_1^2 + \phi_2^2 + \phi_3^2 + \phi_4^2 + 2(\phi_1\phi_3 + \phi_2\phi_4 - \phi_1\phi_4 - \phi_3\phi_2 - \phi_1\phi_4 - \phi_2\phi_3) \rangle}$$

and employing the definition

$$(25) \quad \phi_0^2 \rho_{\phi}(\vec{r} + \vec{x}'' - \vec{x}') = \langle \phi(\vec{x} + \vec{x}') \phi(\vec{x} + \vec{x}'' + \vec{r}) \rangle$$

where $\rho_{\phi}(\vec{x})$ is the phase auto-correlation function ($\rho_{\phi}(0)$ equals unity) and ϕ_0 is the variance of $\phi(\vec{x})$ we have

$$(26) \quad \langle e^{i(\phi_1 - \phi_2 + \phi_3 - \phi_4)} \rangle = e^{-\phi_0^2 f}$$

where

$$(27) \quad f = 2 + \rho_{\phi}(\vec{x}_{31} + \vec{r}) + \rho_{\phi}(\vec{x}_{24} + \vec{r}) - \rho_{\phi}(\vec{x}_{12}) - \rho_{\phi}(\vec{x}_{34}) - \rho_{\phi}(\vec{x}_{14} + \vec{r}) - \rho_{\phi}(\vec{x}_{23} + \vec{r})$$

and

$$(28) \quad \chi_{ij} = \vec{x}_i - \vec{x}_j$$

So

$$(29) \quad m_{\rho_I}^2(\vec{r}) + 1 = \left(\frac{k_0}{2\pi L}\right)^4 \iiint\limits_{\mathcal{V}} da_1 da_2 da_3 da_4 e^{-\frac{i k_0}{2L}(\vec{x}_1^2 - \vec{x}_2^2 + \vec{x}_3^2 - \vec{x}_4^2)} e^{-\phi_0 f}$$

As it stands, this integral is intractable; however, as we are considering the case of weak scattering, the phase deviation ϕ_0 is much less than unity, so $e^{-\phi_0^2 f}$ can be expanded to $1 - \phi_0^2 f$ and

$$(30) \quad m_{\rho_I}^2(\vec{r}) + 1 \simeq \left(\frac{k_0}{2\pi L}\right)^4 \iiint\limits_{\mathcal{V}} da_1 da_2 da_3 da_4 (1 - \phi_0^2 f) e^{-\frac{i k_0}{2L}(\vec{x}_1^2 - \vec{x}_2^2 + \vec{x}_3^2 - \vec{x}_4^2)}$$

For mathematical simplicity, we go to the one dimensional case, where we can apply relation (22) directly. (Otherwise, we could re-write f in terms of auto-correlation functions of x_i and y_i , the cartesian components of \vec{x}_i , and proceed essentially as follows)

$$(31) \quad m_{\rho_I}^2(r) + 1 = \left(\frac{k_0}{2\pi L}\right)^2 \iiint\limits_{\mathcal{V}} dx_1 dx_2 dx_3 dx_4 (1 - \phi_0^2 f) e^{-\frac{i k_0}{2L}(x_1^2 - x_2^2 + x_3^2 - x_4^2)}$$

using relation (22) repeatedly, the result becomes

$$(32) \quad m_{\rho_I}^2(r) = -\left(\frac{k_0 \phi_0}{2\pi L}\right)^2 \iiint\limits_{\mathcal{V}} dx_1 dx_2 dx_3 dx_4 \left[\rho_{\phi}(r+x_3-x_1) + \rho_{\phi}(r+x_4-x_2) \right] \\ \cdot e^{\frac{i k_0}{2L}(x_1^2 - x_2^2 + x_3^2 - x_4^2)} + 2\phi_0^2 \left(\frac{k_0}{2\pi L}\right) \iiint\limits_{\mathcal{V}} dx_1 dx_2 \rho_{\phi}(r) \cos \frac{k_0}{2L}(x_1^2 - x_2^2)$$

$$(33) \quad = -\left(\frac{k_0 \phi_0}{2\pi L}\right)^2 \iiint\limits_{\mathcal{V}} dx_1 dx_2 dx_3 dx_4 \left[\rho_{\phi}(r+x_3-x_1) + \rho_{\phi}(r+x_4-x_2) \right] e^{\frac{i k_0}{2L}(x_1^2 - x_2^2 + x_3^2 - x_4^2)} \\ + 2\phi_0^2 \rho_{\phi}(r)$$

$$(34) \quad \equiv I + \phi_0^2 \rho_{\phi}(r)$$

Now Fourier transform both sides:

$$(35) \quad F_I(K) = 2 F_\phi(K) + \mathcal{H.T.}(I)$$

applying the shift theorem as in (Bracewell, 1965, p. 104) one finds that

$$(36) \quad \int \rho_\phi(r+x'-x'') e^{iKr} dr = F_\phi(K) e^{-iK(x''-x')}$$

so

$$(37) \quad \mathcal{H.T.}(I) \longrightarrow -2 F_\phi(K) \iint dx_1 dx_2 \frac{k}{2\pi L} e^{\frac{ik_0}{2L}(x_1^2+x_2^2) + iK(x_1-x_2)}$$

Changing variables to

$$(38) \quad x_1' = x_1 + \frac{KL}{k_0}, \quad x_2' = x_2 - \frac{KL}{k_0}$$

gives

$$(39) \quad \mathcal{H.T.}(I) = -2 F_\phi(K) e^{i \frac{K^2 L}{k_0}}$$

so we have

$$(40) \quad F_I(K) = 2 F_\phi(K) \left(1 - e^{i \frac{K^2 L}{k_0}}\right)$$

But the intensity fluctuations are real, we take the real part and

$$(41) \quad F_I(K) = 2 F_\phi(K) \left(1 - \cos \frac{K^2 L}{k_0}\right)$$

$$(42) \quad = 4 F_\phi(K) \sin^2 \left(\frac{K^2 L}{2k_0}\right)$$

where $F_\phi(q)$ is the spatial power spectrum of the phase irregularities. This spectrum is the same on the ground as it is

at the exit plane of the slab (Cronyn, 1970). Note that

$$(43) \quad F_{\phi}(K) = \mathcal{F} \cdot \mathcal{T} \cdot \left\{ \phi_o^2 \rho_{\phi}(\vec{r}) \right\}$$

Following Cronyn (1970)

$$(44) \quad \phi_o^2 \rho_{\phi}(\vec{r}) = k_o^2 \left\langle \int_0^{\Delta L} dz_1 \int_0^{\Delta L} dz_2 \delta n(\xi, \eta, z_1) \delta n(\xi + \xi_o, \eta + \eta_o, z_2) \right\rangle$$

$$(45) \quad = (r_e \lambda)^2 \left\langle \int_0^{\Delta L} dz_1 \int_0^{\Delta L} dz_2 \delta N_e(\xi, \eta, z_1) \delta N_e(\xi + \xi_o, \eta + \eta_o, z_2) \right\rangle$$

where r_e is the classical electron radius, λ is the wavelength of the incident radiation, and ΔL is the thickness of the region.

$$(46) \quad \phi_o^2 \rho_{\phi}(\vec{r}) = (r_e \lambda)^2 \int_0^{\Delta L} dz_1 \int_0^{\Delta L} dz_2 \left\langle \delta N_e(\xi, \eta, z_1) \delta N_e(\xi + \xi_o, \eta + \eta_o, z_2) \right\rangle$$

$$(47) \quad = (r_e \lambda)^2 \int_0^{\Delta L} dz_1 \int_0^{\Delta L} dz_2 (\Delta N_e)^2 \rho_{N_e}(\vec{r}, z_1 - z_2)$$

Let ℓ_z be the scale for which $\rho(|z_1 - z_2|)$ is very small if $|z_1 - z_2|$ is greater than ℓ_z ; now assume ℓ_z is much less than ΔL (valid in this case). Then the limits on the second integral can be extended to infinity with an error on the order of $\ell_z/\Delta L$. Thus, with the coordinate transformation $z_1 - z_2$ going to L we have

$$(48) \quad \phi_o^2 \rho_{\phi}(\vec{r}) \cong (r_e \lambda)^2 (\Delta N_e)^2 \int_{-L}^{-L+\Delta L} dz_2 \int_{-\infty}^{\infty} dL \rho_{N_e}(\vec{r}, L)$$

$$(49) \quad = (r_e \lambda)^2 (\Delta N_e)^2 \Delta L \int_{-\infty}^{\infty} dL \rho_{N_e}(\vec{r}, L)$$

Now

$$(50) \quad F_{N_e}(k_x, k_y, k_z) = (2\pi)^{-3} \iint d^2r dL (\Delta N_e)^2 \rho_{N_e}(\vec{r}, L) e^{-ik_z L} e^{-ik_x x} e^{-ik_y y}$$

where k_x, k_y, k_z are components of the 3-D spatial wave vector

$$(51) \quad \vec{K} \equiv \vec{k} + \hat{L} k_z$$

and

$$(52) \quad F_{N_e}(k_x, k_y, 0) = (2\pi)^{-3} \iint d^2r dL (\Delta N_e)^2 \rho_{N_e}(\vec{r}, L) e^{-i\vec{k} \cdot \vec{r}}$$

So taking the Fourier transform of both sides of (49)

$$(53) \quad F_\phi(\vec{k}) = 2\pi \Delta L (r_e \lambda)^2 F_{N_e}(\vec{k}, 0)$$

and

$$(54) \quad F_I(\vec{k}) = 4 F_\phi(\vec{k}) \sin^2\left(\frac{k^2 \lambda L}{4\pi}\right)$$

However, in actual single receiver observation, one observes a temporal power spectrum which is a one-dimensional cut through the two-dimensional power spectrum, produced as the diffraction pattern is convected through the line of sight by the solar wind. Thus with the solar wind moving in the \hat{x} direction, k_x goes to $2\pi\nu/V_\perp$. So

$$(55) \quad F_I(\nu) = \frac{2\pi}{V_\perp} \int_{-\infty}^{\infty} dk_y F_I\left(\frac{2\pi\nu}{V_\perp}, k_y\right)$$

$$(56) \quad F_I(\nu) = (2\pi r_e \lambda)^2 \frac{\Delta L}{V_\perp} \int_{-\infty}^{\infty} dk_y F_{N_e}\left(\frac{2\pi\nu}{V_\perp}, k_y, 0\right) 4 \sin^2\left(\frac{\left[\frac{2\pi\nu}{V_\perp}\right]^2 + k_y^2}{k_f^2}\right)$$

where k_f^2 equals $4\pi/\lambda L$, k_f is the Fresnel wave number, the wave number associated with the radius of the first Fresnel zone.

This is the result for the temporal spectrum produced by a thin slab of medium in the limit of weak scattering, for a point source. This theory has been extended by Young (1971) to include extended media. The technique is simply to integrate the thin-screen result along the line of sight. The thin-screen result was justified by the geometry of the density irregularity distribution in the medium. So $F_I(\nu)$ is proportional to $\langle \delta N_e^2 \rangle$, and it is assumed that δN_e is proportional to \bar{N}_e which is assumed proportional to $\rho^{-\tau}$, where ρ is heliocentric distance and τ is approximately equal to 4. Under these assumptions, for elongation angles less than 90° , the main contribution to the spectrum comes from a fairly localized region centered about the closest approach to the sun of the line of sight. The extended medium theory removes the restriction of that assumption. This is especially important when considering Fresnel and source size effects, as well as large elongation angles. These considerations will be dealt with more completely in the next section.

It should be emphasized that this theory is valid only in the weak-scattering regime. As one approached smaller elongation angles, the power in the electron density fluctuation spectrum increases, until it reaches a point where there is appreciable strong-scattering. This transition can be recognized as a broadening of the spectrum, with more power being shifted into the higher frequencies. It is also the point of which the weak-scattering theory will no longer produce plausible fits to the data.

B. For Power Law Spectrum

Of main interest is dP , the contribution to the power spectrum of the intensity fluctuations detected at a radio telescope from electron density fluctuations in the interval dL along the line of sight: i.e., it is the differential intensity fluctuation energy between ν and $\nu + d\nu$ contributed by a slab of thickness dL where ν is the frequency of the density fluctuations (ν equals $V_{\perp}/2\pi k_x$). In the thin-screen, weak-scattering approximation for a screen of thickness dL at a distance L from the observer (Cronyn, 1970; Young, 1971)

$$(57) \quad dP = \frac{dL}{V_{\perp}} (2\pi r_e \lambda)^2 \int_{-\infty}^{\infty} dk_y F(k_x, k_y) 4 \sin^2\left(\frac{k_{\perp}^2}{k_f^2}\right) R(\beta, k_{\perp})$$

where r_e is the classical radius of the electron, λ is the observing wave-length, $F(k_x, k_y)$ is the two-dimensional spatial density irregularity power spectrum in the screen for wave number k_x, k_y perpendicular to the earth-source line so that k_{\perp}^2 equals $k_x^2 + k_y^2$. The k_x direction is along the component of screen velocity (V_{\perp}) transverse to the line of sight and the k_y direction perpendicular to both V_{\perp} and the line of sight. The Fresnel filtering function $4 \sin^2(k_{\perp}/k_f)^2$ is characterized by the Fresnel wave number k_f which equals $(4\pi/\lambda L)^{1/2}$. The source visibility function, R , accounts for the finite size of the radio source. R is the Fourier transform of the source brightness distribution (Salpeter, 1967).

We assume

$$(58) \quad F(k_x, k_y, k_z=0) = F_0 (\gamma k_x^2 + k_y^2)^{-q/2}$$

where $\sqrt{\gamma}$ is the axial ratio of the irregularities in phase space. This assumption is supported by spacecraft data (Unti et al., 1973), angular scattering measurements (Cronyn and Mitchell, 1974), and consistent with observed interplanetary scintillation (IPS) spectra (Cronyn, 1972; and Jokipii and Hollweg, 1970). The power law slope (q) is assumed to be $3 < q \leq 4$, again supported by Unti et al. (1973), and Cronyn, 1970. The source visibility is represented by the function

$$(59) \quad R(\beta, k_1, k_x, k_y) = \exp \left[(-\beta k_x^2 - k_y^2) / 2k_1^2 \right]$$

which assumes an elliptical source with a Gaussian brightness distribution, where $\sqrt{\beta}$ is the axial ratio of the source (or rather the axial ratio of the axes of the source as projected in the \hat{x} and \hat{y} directions), and k_1 is $1/L\Omega$, where L is the distance to the scattering region and Ω is the angular scale (diameter to the $1/e$ point) of the source. Note that for sources out of the ecliptic plane, the largest (or smallest) axial ratio measured over a period of a year (assuming daily measurements) should represent the true axial ratio of the source, to the extent that the source can be considered to be an ellipse. This is due to the geometry--at least once a year, both the major and minor axes of the source (each at different time) will line up with the projected solar wind velocity vector.

Note that we are ignoring the inner and outer scales of the irregularities, except where the outer scale, k_0 , occurs in the "constant" F_0 , as defined in the density irregularity auto-correlation function. From the angular scattering measurements (Cronyn and Mitchell, 1974) and satellite data (Cronyn, 1970) the outer scale is always much greater than the Fresnel scale, and so does not affect the shape of the spectrum in the IPS range, while the inner scale is less than .3 km, or well below the scales (≥ 40 km) which contribute significant power to the fluctuations.

We can now write

$$(60) \quad dP = \frac{dL}{V_1} (2\pi r_e \lambda)^2 F_0 \int_0^\infty dk_y (\gamma k_x^2 + k_y^2)^{-\frac{q}{2}} \sin^2\left(\frac{k_x^2 + k_y^2}{k_f^2}\right) e^{-\frac{\beta k_x^2 + k_y^2}{2k_f^2}}$$

Defining a new function to temporarily remove the constants, we have

$$(61) \quad dP = \frac{dL}{V_1} (2\pi r_e \lambda)^2 F_0 \Gamma\left(\frac{1}{2}\right) k_f^{1-q} J(s, \gamma, \beta, \rho, s_1)$$

where

$$(62) \quad S \equiv k_x^2 / k_f^2, \quad S_1 \equiv k_i^2 / k_f^2$$

and

$$(63) \quad F_0 \approx \frac{\langle \Delta N_e^2 \rangle \Gamma\left(\frac{q}{2}\right)}{\pi \Gamma\left(\frac{1}{2}\right) \Gamma\left(\frac{q-3}{2}\right)} k_0^{q-3}$$

(see Appendix A). By the derivation shown in Appendix B, an analytic expression for J is

$$(64) \quad J(s, \gamma, \beta, \rho, s_1) = e^{-\frac{\beta S}{2S_1}} (\gamma S)^{\frac{1-q}{2}} \left[U\left(\frac{1}{2}, \frac{3-q}{2}, \frac{\gamma S}{2S_1}\right) - \mathcal{R}_e \left\{ e^{i2S} U\left(\frac{1}{2}, \frac{3-q}{2}, \frac{\gamma S}{2S_1} - 2i\gamma S\right) \right\} \right]$$

where U is a confluent hypergeometric function (Abramowitz and Stegun, 1964). Although J is analytic, it does not lend itself to quick hand calculations. In general, J must be treated numerically; however, in certain limiting cases of its arguments, it can be approximated by fairly simple expansions. Evaluation of this function is left to the next chapter.

CHAPTER III

NUMERICAL TECHNIQUE

A. Expansion of J Function

In this chapter, we wish to find expansions for the J function, defined in equation (64). These expansions are obtained by expanding each of the two confluent hypergeometric functions (CHF) separately and keeping the first few terms in each expansion. In the range of small (less than unity) arguments of the CHF, the defining power series expansion is used. This series is given in Appendix A. For large arguments, an asymptotic expansion is used (see Appendix B) which for the parameter values we are using converges more rapidly than the asymptotic expansion given in Abramowitz and Stegun, 1964. See Figures 2a and 2b for error contours of this expansion.

Using these two expansions, we can develop three expansions for the J function which cover the entire complex plane of its argument with very little error (see Figures 3a, 3b and 3c). The error is less than ten percent over most of the plane, slightly exceeding ten percent in the troughs of the "Fresnel ripple". This ripple will be discussed later, but for now it will suffice to say that the error in the troughs is of little significance in the final model spectra, and the error in these final spectra is ten percent at the worst. This error is quite acceptable, for several reasons. First, the error is large only in a limited range, and the function can be fit to experimental spectra in the areas where

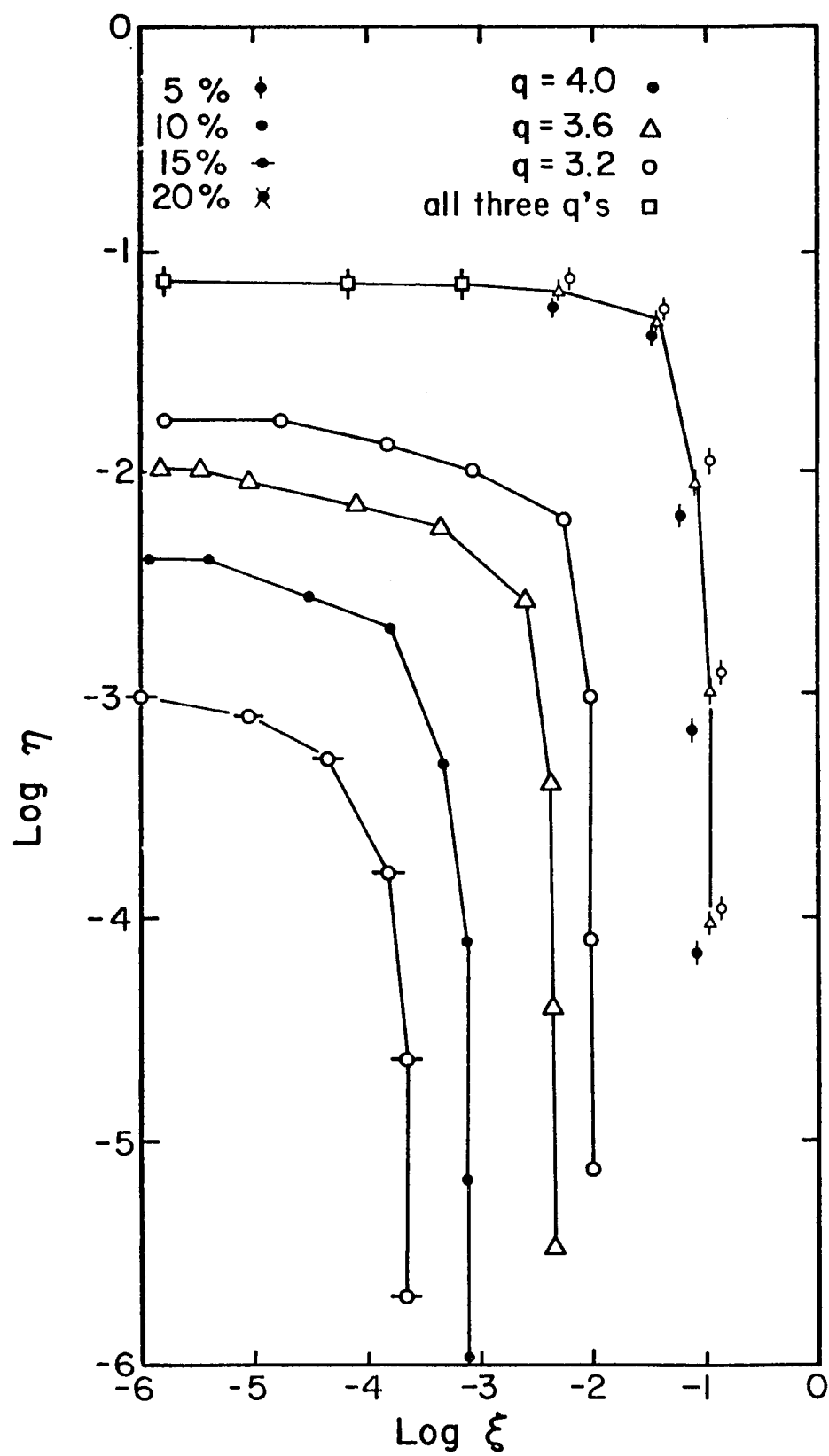


FIGURE 2a

Contours of the asymptotic expansion of the real part of the confluent hypergeometric function $U(\frac{1}{2}, \frac{3-q}{2}, \xi + i\eta)$ in the logarithmically spaced $\xi - \eta$ complex plane.

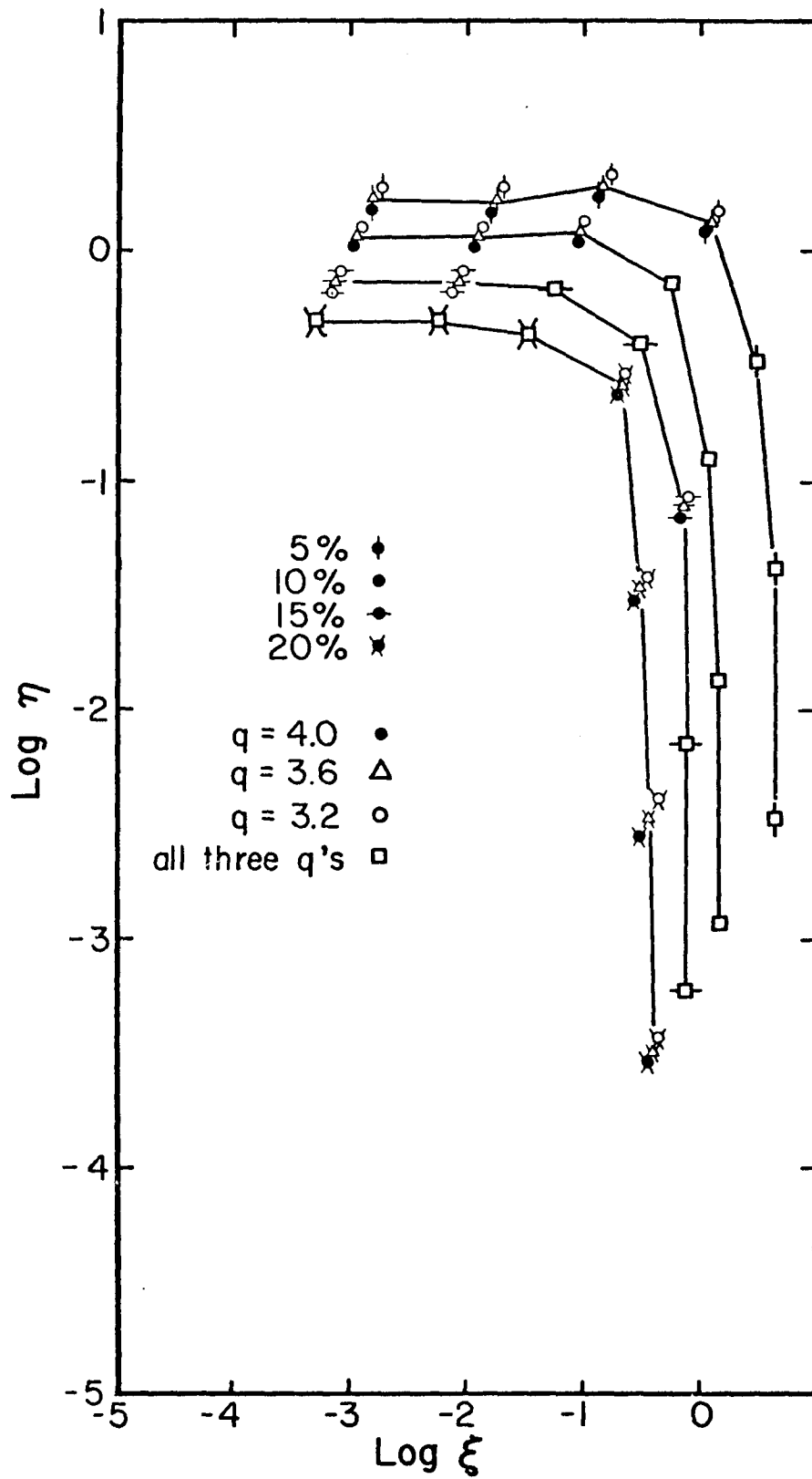


FIGURE 2b

Same as Figure 2a, for the imaginary part of U .

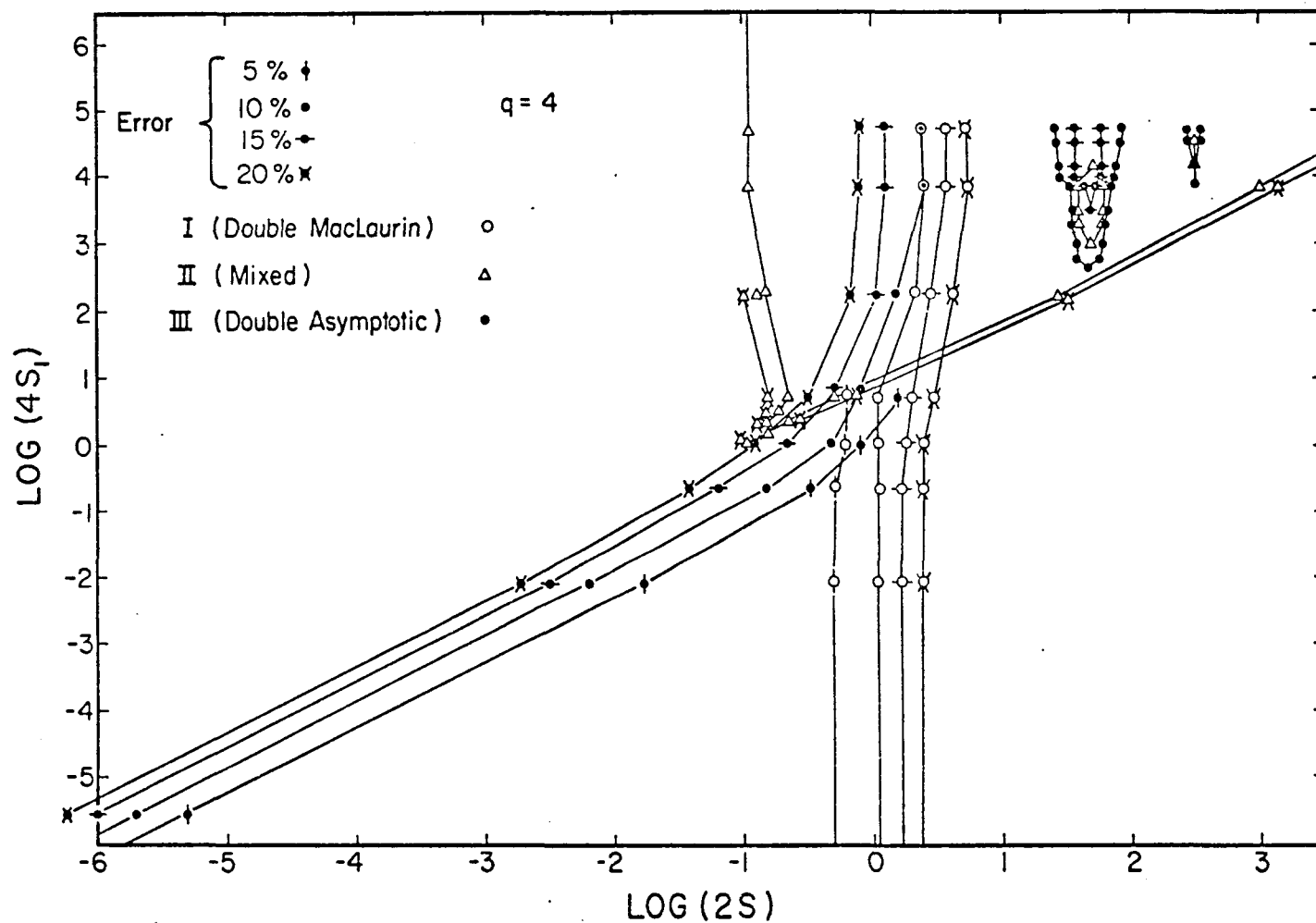


FIGURE 3a

Error plot of J function in the $\log (2S)$ vs $\log (4S_1)$ plane, for power law index (q) equal to 4. S is proportional to the frequency of the intensity fluctuation squared (ν^2), and S_1 is proportional to the frequency corresponding to the source angular size squared.

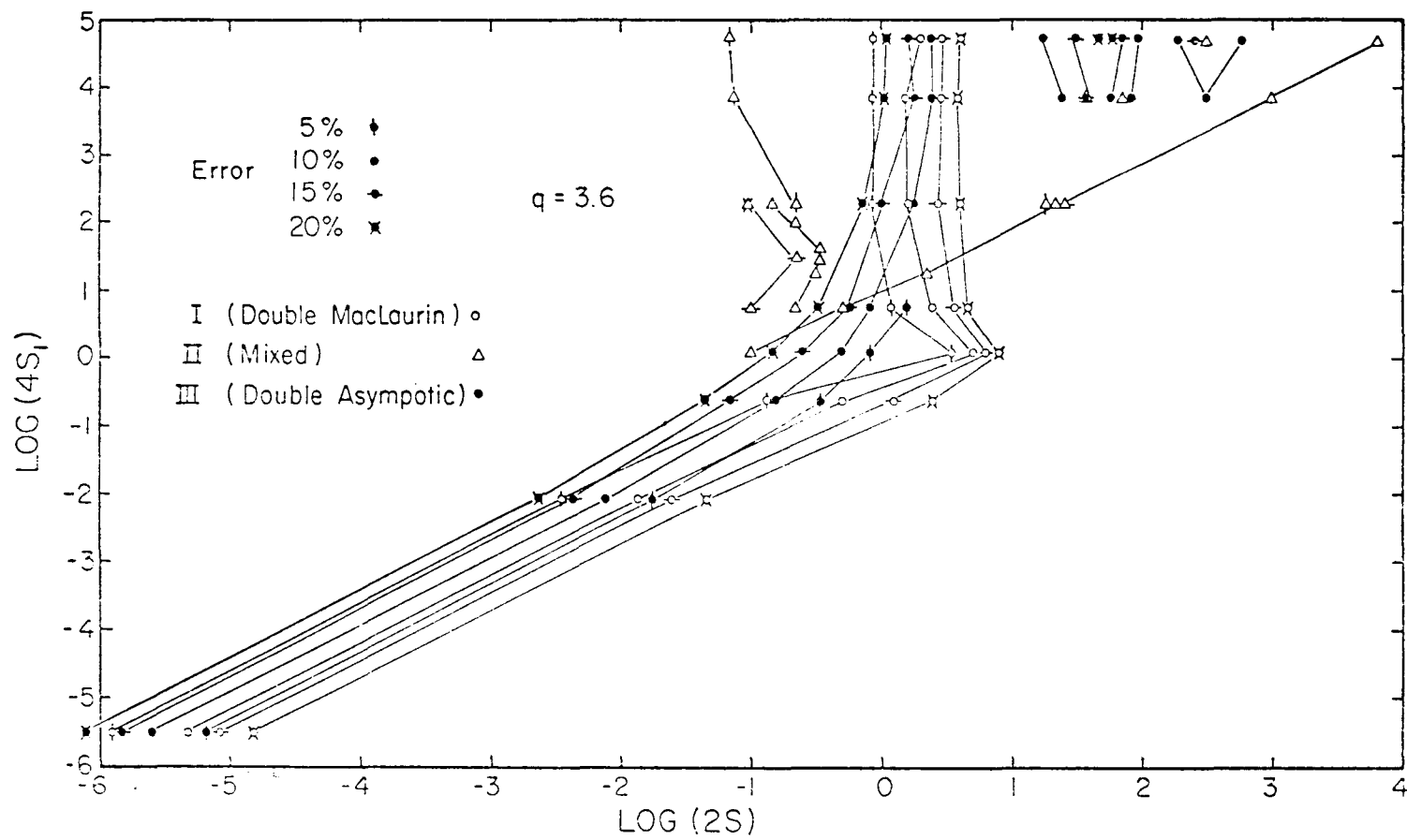


FIGURE 3b

Same as Figure 3a, with q equal to 3.6

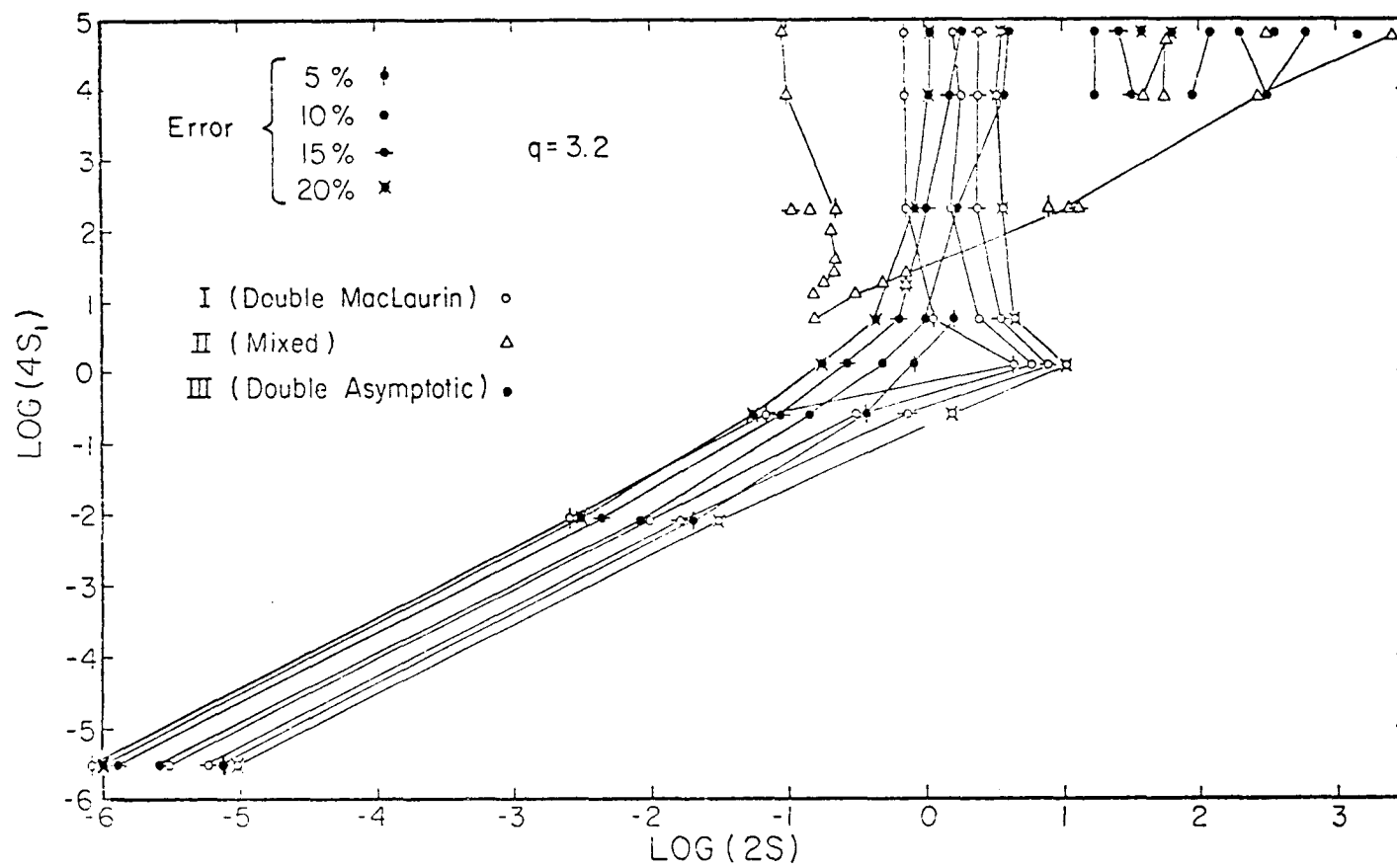


FIGURE 3c

Same as 3a, with q equal to 3.2

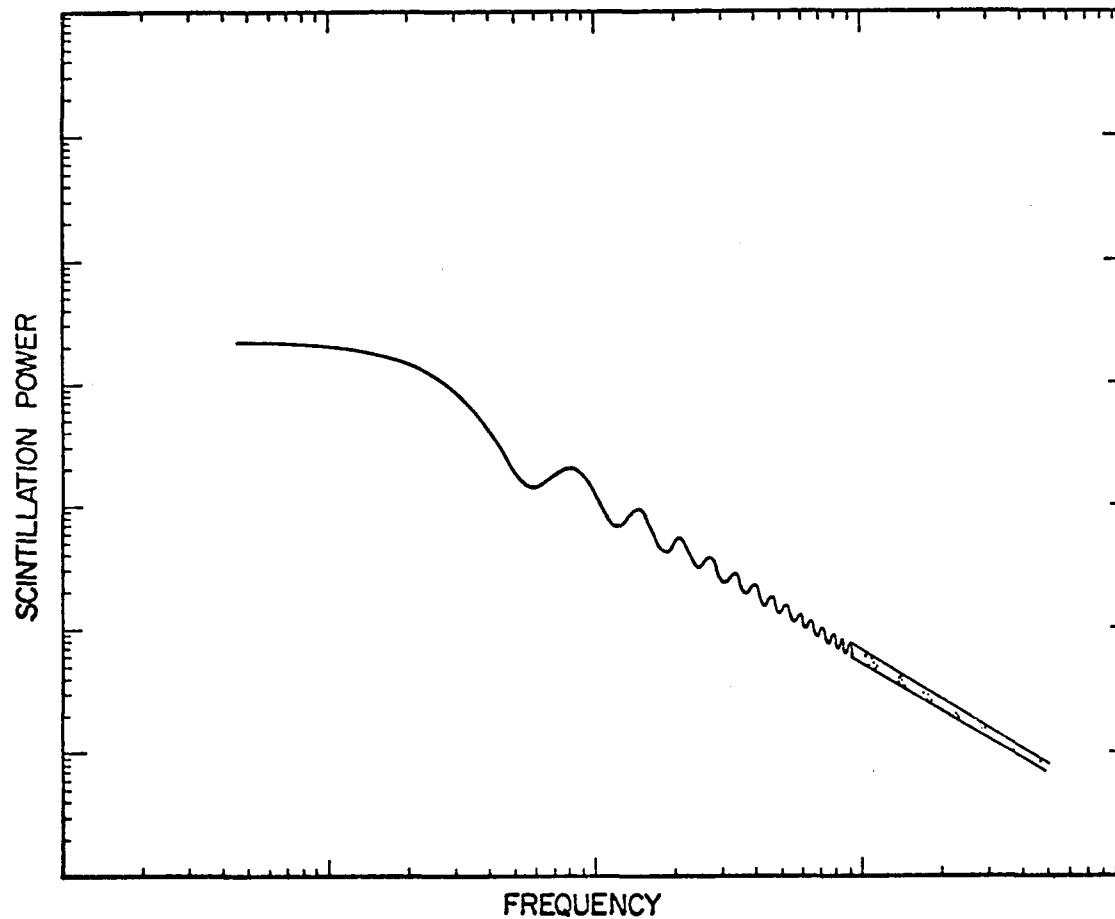


FIGURE 4

Thin slab, point source theoretical spectrum shown on an arbitrary log-log scale. Points of note are the Fresnel turn over to a flattening of lower frequencies, and the Fresnel ripple imposed on the power law at higher frequencies.

the error is low, with accuracy. Second, other assumptions made in obtaining the final spectra are probably cruder than ten percent accuracy; nevertheless, reasonable fits can be made to the data. Third, the data itself, in most cases, fluctuates statistically by more than ten percent as can be seen in the comparison to the data, (see Figures 9a and 9b). This fluctuation can be attributed to temporal fluctuations of the medium over the observation time, lack of time resolution in the instrument, and deviation of the geometry of the turbulent region from that idealized in the model.

So in the expansions for J we have reasonable approximations for generating model spectra of scattering from a thick slab of the interplanetary medium. Figure 4 is an example of how a thin screen, point source spectrum appears.

The three expansions follow. The range of these expansions is found by choosing that expansion with the smallest error at any given point in the complex plane of the arguments, as can be determined from Figure 3a, 3b and 3c.

$$\begin{aligned}
 E_I = 2^{\frac{\ell-1}{2}} & \left[\frac{4 \Gamma(\frac{\ell-1}{2})}{(1-1)(\ell-3) \sqrt{\pi}} \left((4S_1)^{\frac{\ell-1}{2}} - \left(\frac{1}{16S_1^2} + 1 \right)^{\frac{\ell-1}{4}} \left\{ \cos \frac{\ell-1}{2} \theta + 2S \sin \frac{\ell-1}{2} \theta \right\} + \frac{2\ell S \ell}{\ell+1} \left\{ (4S_1)^{-\frac{\ell+1}{2}} \right. \right. \right. \\
 (65) \quad & \left. \left. \left. - \left(1 + \frac{1}{16S_1^2} \right)^{\frac{\ell+1}{4}} \cos \frac{\ell+1}{2} \theta \right\} \right) + \frac{\Gamma(\frac{\ell-1}{2})}{\Gamma(\frac{\ell}{2})} (2\ell S)^{\frac{\ell-1}{2}} \left\{ \frac{1}{2\ell^2} + \frac{1}{(\ell-3)\ell} + \frac{3}{2(\ell-3)(\ell-5)} \right\} \right], \\
 \Theta = \tan^{-1} 4S_1
 \end{aligned}$$

$$\begin{aligned}
 E_{II} = & \left\{ \Gamma(\frac{\ell-1}{2}) / \Gamma(\frac{\ell}{2}) - \cos(2S + \theta_0/2) \omega_{02}^{-\frac{1}{2}} - .375 \ell/2 \cos(2S + 2.5\theta_1) \omega_{12}^{-2.5} \right. \\
 & - .3125 \ell/2 \cos(2S + 3.5\theta_1) \omega_{12}^{-3.5} - .2734375 \ell/2 \cos(2S + 4.5\theta_1) \omega_{12}^{-4.5} \\
 (66) \quad & \left. - .8203125 \ell(\ell-1)/4 \cos(2S + 4.5\theta_2) \omega_{22}^{-4.5} \right\} (\ell S)^{\frac{\ell-1}{2}},
 \end{aligned}$$

(67)

$$E_{\text{III}} = E_{\text{II}} - (\gamma S)^{\frac{1-q}{2}} \left[\frac{\Gamma(\frac{q-1}{2})}{\Gamma(\frac{q}{2})} - \left\{ \omega_{01}^{-\frac{1}{2}} + .375 \, q/2 \, \omega_{11}^{-2.5} + .3125 \, q/2 \, \omega_{11}^{-3.5} \right. \right. \\ \left. \left. + .2734375 \, q/2 \, \omega_{11}^{-4.5} + q(q-1) .8203125/4 \, \omega_{21}^{-4.5} \right\} \right],$$

$$\omega_{n1} = \frac{2\gamma S}{4S_1} + n + q/2 \quad \omega_{n2} = \left\{ (2\gamma S)^2 + \left(\frac{2\gamma S}{4S_1} + n + q/2 \right)^2 \right\}^{1/2}$$

$$\theta_n = \tan^{-1} \left(\frac{2\gamma S}{2\gamma S/4S_1 + n + q/2} \right)$$

Expansion (I) is in the small argument range of both CHF, and as the errors in both CHF are of the same sign, they tend to be minimized in the J function which essentially takes the difference between the two CHF. This is true also of the expansion in region III, where both CHF are in the asymptotic range and again the error is minimized.

In region II, however, the CHF are not both in the same expansions. One is in the small argument range, while the other is in the asymptotic range. Their errors thus have different functional dependence on the arguments, and do not subtract. For this reason, the greatest accuracy was obtained by keeping only the lowest order terms in the CHF expansion for small arguments; adding the next order term to the expansion increases the error.

B. Integration over Extended Medium

In the interplanetary medium, however, we have not a thin but an extended scattering medium. Thus we must integrate our thin screen result over a series of slabs along the line of sight through the medium. Both J and some of the "constants" multiplying J to obtain dP/dL are functions of

distance from the observer, L , and elongation angle, ϵ . The integration must be performed numerically. Rather than integrating over fixed increments in L for a given ϵ , a series of L 's were chosen by approximating crudely the contribution to the scattering from each point along the line of sight (assuming the scattering to be proportional to ρ^{-4}), and using those L 's corresponding to slabs of approximately equal scattering power. This process permitted a reduction in the number of calculations necessary, and cut down the computer time.

The end result of this is a thick-screen, weak-scattering model spectrum for the case of a uniform medium. Regions of increased turbulence can be easily accommodated in the theory by weighting a given L value in the integration along the line of sight. Thus stream-stream interaction regions and blast waves, as well as rarifactions, can be modeled.

C. Scintillation Index and Scale

Further useful results are obtained through integrating the spectrum over frequency to obtain the zeroth moment (known as the scintillation index) and the second moment, both of which are observables and more easily obtainable experimentally than a full spectrum. This integration is performed using a modified Simpson's Rule integration, which accommodates a logarithmically incremented abscissa. This is accomplished by changing the increment along the frequency axis by a multiplicative constant as you move along the axis. The algorithm

would be set up as follows:

(68)

$$\int_{\nu_1}^{\nu_N} f(\nu) d\nu \rightarrow \sum_{n=1,3,5,\dots}^{N-2} \left\{ \left[(f_n + f_{n+2})/2 + 2 f_{n+1} \right] / 3 \right\} \{ (\alpha^2 - 1) \nu_n \}$$

where

$$(69) \quad \nu_n = \alpha \nu_{n-1}, \quad \alpha > 1$$

and f_n is any well behaved function $f(\nu_n)$. Plots of scintillation index and second moment versus elongation angle are presented in Figures 5 and 6. These figures will be discussed further in the next chapter. Those curves labeled "band-passed" were produced by integrating the spectrum from .1 Hz to 1.5 Hz; those labeled "complete" were produced by integrating the spectrum from .01 Hz to 10 Hz. The integration limits for the theoretical curves approximate zero to infinity well for the index curves, but not for the second moment curve for a point source. This is because without the exponential cut off imposed by the source visibility function, the integral to infinity for the second moment would blow up. In actual case, another effect would cut off the spectrum. An inner scale to the turbulence, corresponding to some high frequency, would cut off the spectrum exponentially and thus limit the second moment.

D. Scattering Power Profile

Another result which can be obtained with no extra effort is a breakdown of the thick-screen results into the contributions from the various L values. Figures 7a and 7b

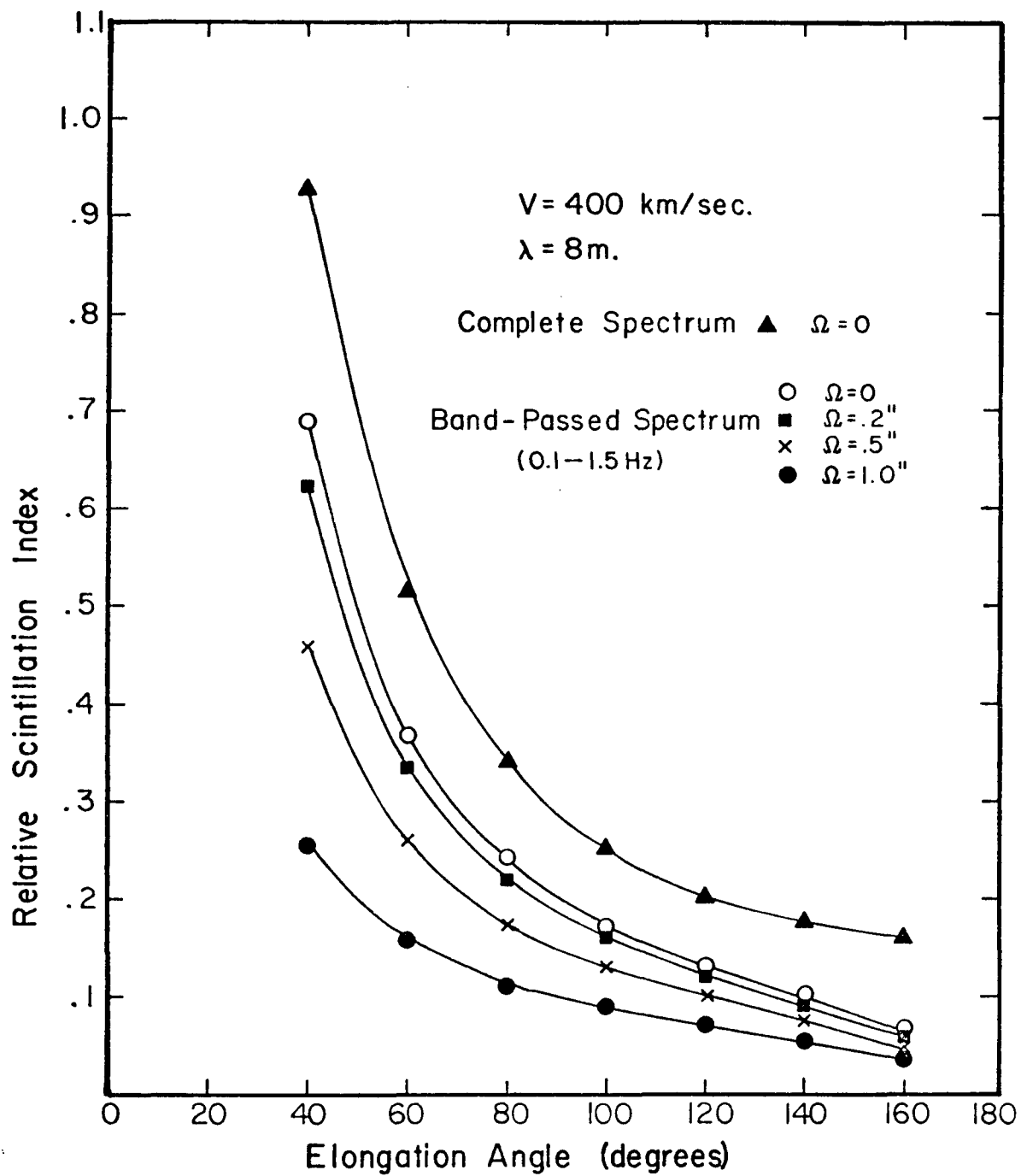


FIGURE 5

Scintillation index vs elongation angle (ϵ) for band-passed and complete spectra, at several source sizes (Ω).

$V = 400 \text{ km/sec, } q = 3.6$

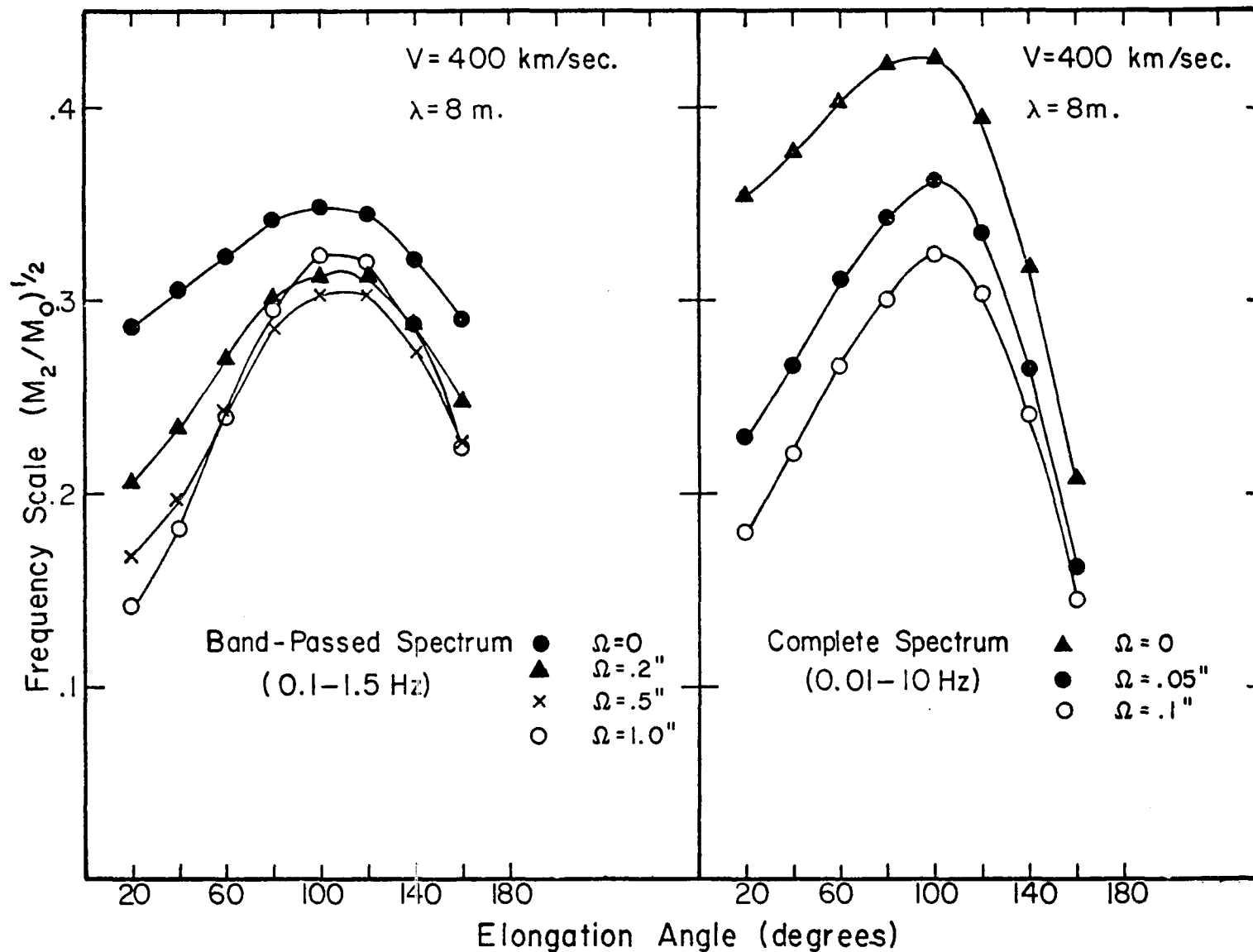


FIGURE 6

Second moment vs elongation angle for band-passed and complete spectra, for several sizes.

$V = 400$ km/sec, $q = 3.6$

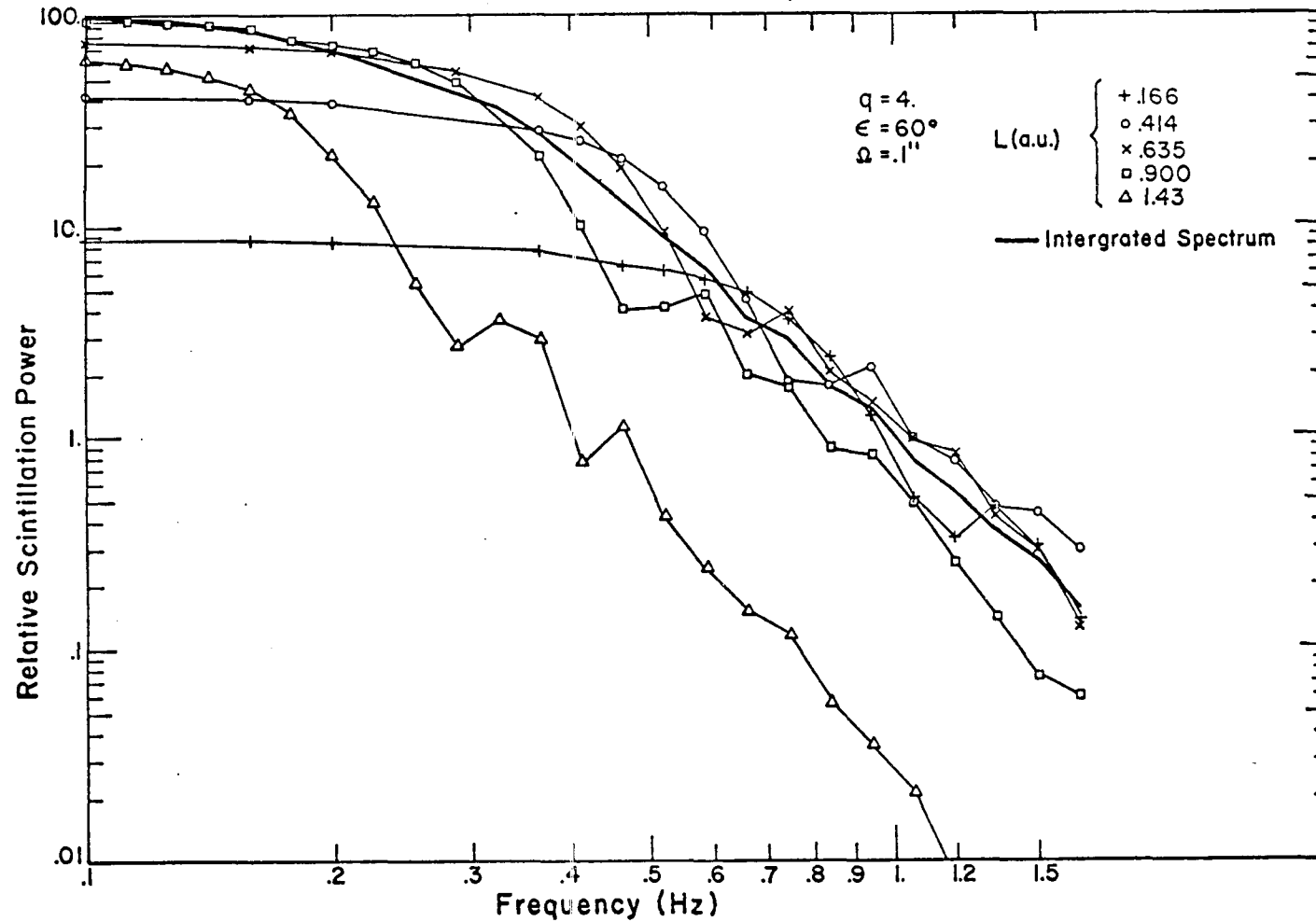


FIGURE 7a

Computed extended medium spectra (heavy line), computed using five different slabs through the quiet medium, for q equal to 4.0. Also shown are the separate spectra for each slab, indicating the relative strength of the scattering at a given frequency for a particular slab. The source size is $\Omega = .1''$, the elongation angle 60° . $V = 600$ km/sec

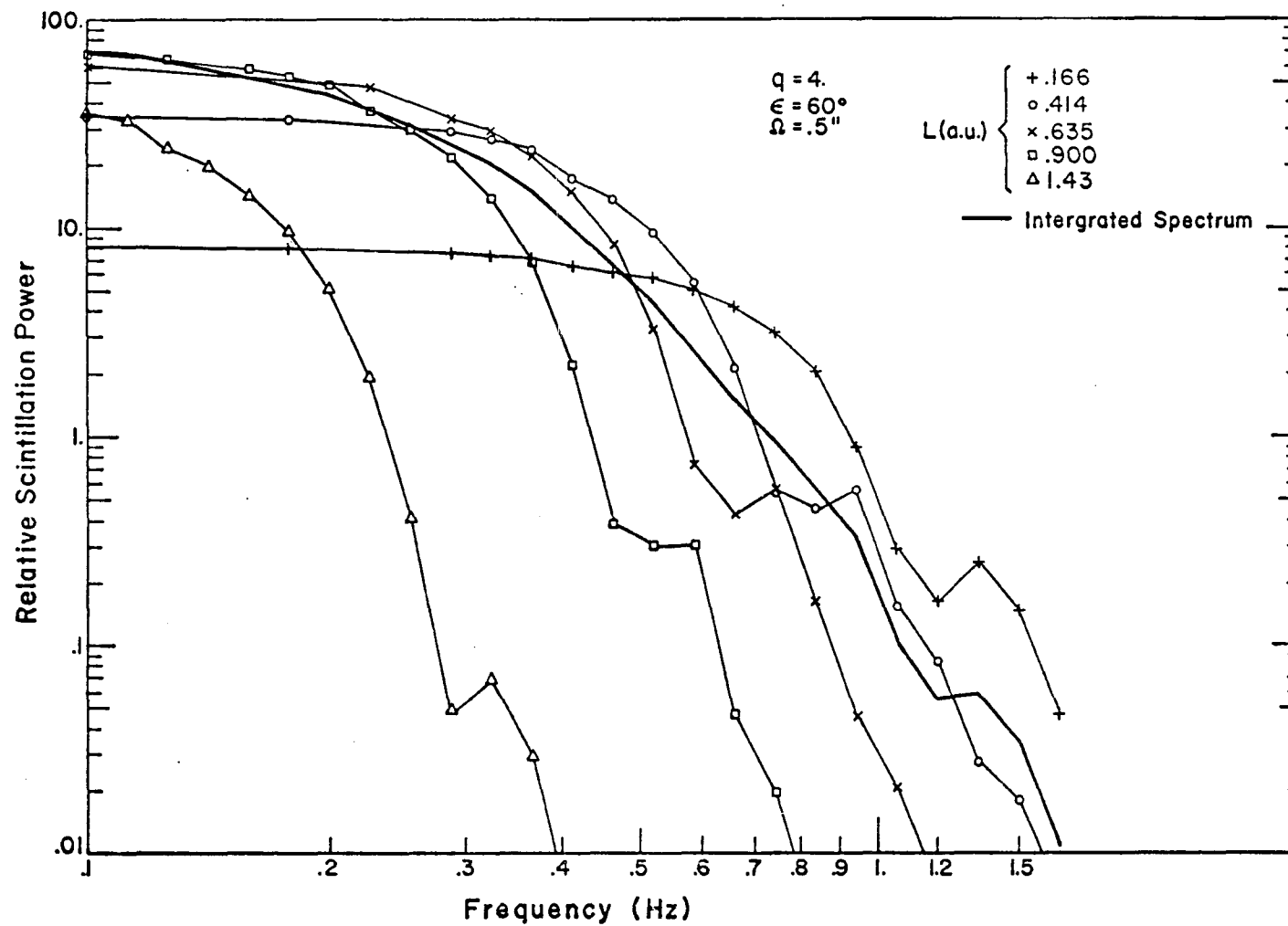


FIGURE 7b

Same as 7a, with $\Omega = .5''$

show a series of spectra corresponding to different L values. This breakdown demonstrates the relative contribution at a given frequency from different parts of the medium. Figure 8 shows the results of integrating each of these spectra over frequency, obtaining the relative contribution from various parts of the medium to the scintillation index.

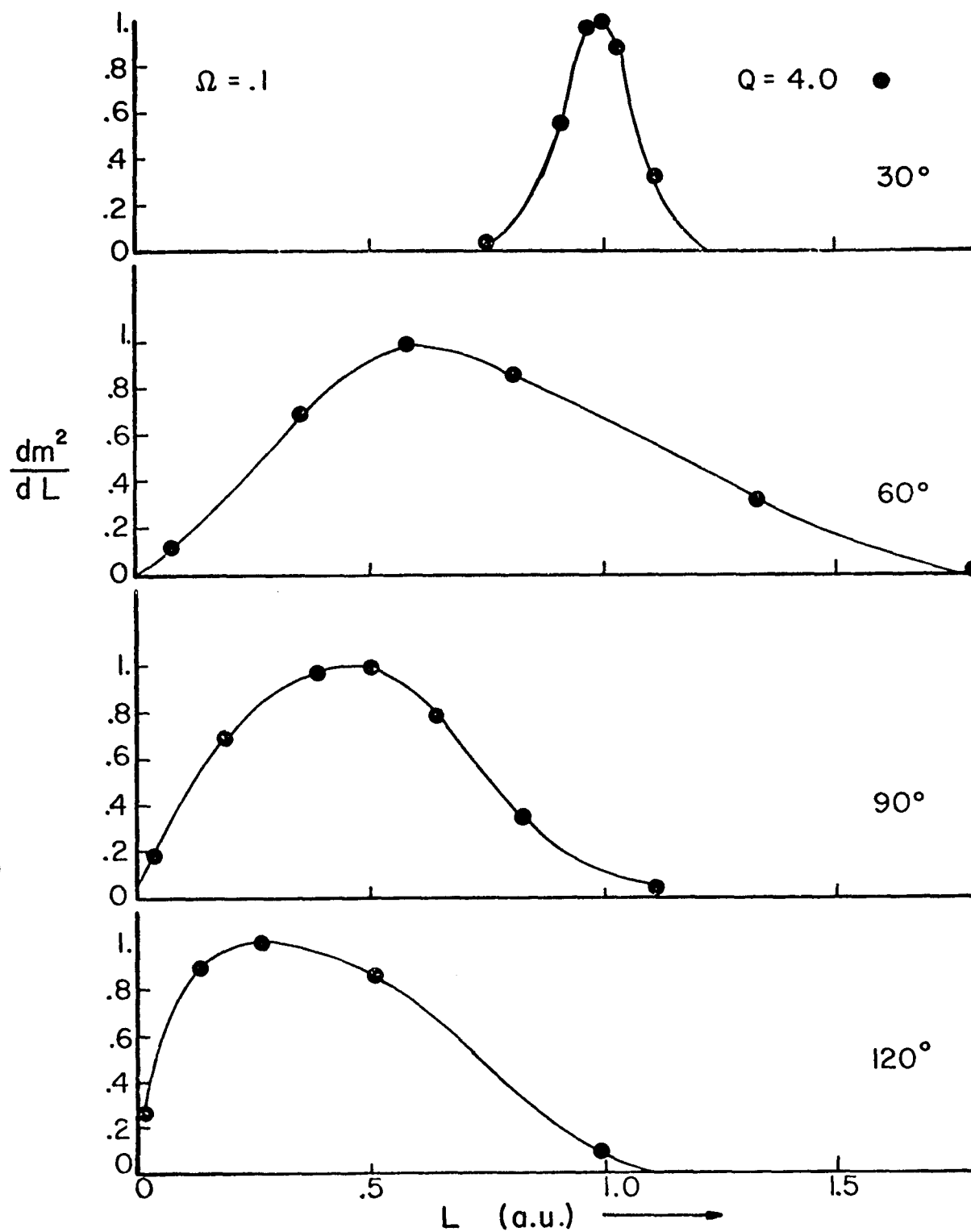


FIGURE 8

Relative contribution to the total scattered intensity from different distances (L 's) along the earth-source line, for different elongation angles (ϵ). Source size is .1"

Velocity is 400 km/sec, $q = 4.0$

CHAPTER IV

DISCUSSION

A. Thin Slab Spectrum

In order to understand the computed spectrum and its moments, let us now examine the scattering qualitatively. We first consider the thin slab case, and then the effect of the integration over many thin slabs.

The most obvious departure of the computed spectrum from the straight power law by which we model the electron density irregularity spectrum is the result of Fresnel diffraction effects. As the slab is at a finite distance from the observer, Fresnel diffraction becomes important. Structure which is larger than the first Fresnel zone has its scattering power severely attenuated. This shows up in the detected spectrum as a flattening for frequencies lower than the Fresnel frequency (the frequency associated with structure of the radius of the first Fresnel zone), (see figure 4). At higher frequencies the power law is observed, but with an exponent reduced by unity due to the strip integration over k_y , and with a quasi-sinusoidal ripple. The ripple is caused by Fresnel diffraction from the second and higher Fresnel zones. Thus, were a thin-screen spectrum observable, one would need only know the solar wind speed to be able to determine the distance to the screen, or vice versa. The other effect distorting the spectrum is the source brightness distribution. Disregarding the source axial ratio, its angular

scale will cause attenuation of the spectrum for frequencies higher than the frequency corresponding to structure in the medium with the angular scale of the source. This would appear as an exponential cut off of the spectrum at high frequencies.

B. Extended Medium Spectrum and Moments

However, thin-screen spectra are rarely, if ever, seen in IPS, so let us go to the thick-screen (extended medium) case. Both the Fresnel effects and the source size effects are functions of distance to the scattering medium. Thus the frequencies at which these effects are seen vary from one slab to the next along the line of sight. The resulting integrated spectrum loses the distinct structure of the thin screen spectra (see Figures 7a and 7b), making identification of the parameters more difficult, and introducing another broad degree of freedom, namely the scattering power profile along the line of sight. For a quiet medium, this profile is shown in Figure 8. In the integrated spectrum, the Fresnel ripple is usually entirely washed out, and the turn-over to the flattening is drawn out (Figures 7a and 7b).

The scintillation index is the integral over the spectrum. This is the total scattered power, and is easily measured. The index varies with source size, and also with elongation, as the scattering power of the turbulence varies with elongation. Likewise, the second moment is a function of source size and elongation. Observation of these two

observables over a period of time for a given source should provide information on both the source and the medium. Spectra taken from time to time would provide more information and help to interpret the observations of index and second moment.

C. Effects of Band-Passing Data

One feature of this model is the ability to include the effects which band-passing of the observations have on the observed index and scale (second moment). This effect is in fact important, as can be seen in Figures 5 and 6. In order to understand the significance of the index and scale, the spectrum itself must be fit and understood in terms of the model. Once an understanding has been reached through examination of spectra, a source can then be observed over a period of months or years using the much simpler data acquisition techniques required for obtaining index and scale.

The effect of band-passing on the index is fairly straight forward. The high-pass filter removes ionospheric scintillation, but also a fraction of IPS. As the observed spectrum is flat as it goes to zero frequency, there is merely a rectangular area under the low frequency end of the spectrum which is lost, and this can be easily calculated. The low-pass filter removes galactic background noise and, as the power is down considerably at this frequency, has little effect on the index. The scale is affected by both filters, however. The second moment is defined as follows.

$$(70) \quad \nu_2 = \left(\int_0^\infty P(\nu) \nu^2 d\nu / \int_0^\infty P(\nu) d\nu \right)^{1/2}$$

So ν_2 is normalized by the scintillation index, and thus is affected because m (index) is affected. Also, the limits on the integrals are not zero to infinity experimentally, but rather ν_H (high pass frequency) to ν_L (low pass frequency). These artificial limits change the shape of the spectrum, and therefore change the second moment. Theoretical analytic expressions can be obtained for both index and scale without first calculating the spectrum, but not for a band-passed spectrum, which is the actual case. Note that for a point source, the theoretical second moment would be infinite; this implies that for very small sources, the second moment reflects only the Fresnel cut off and the low-pass filter cut off. For larger sources, the exponential cut off due to the finite angular diameter of the source will dominate before the low-pass filter, and the second moment can be used to characterize the source size.

D. Fits to Data

Using index and scale to investigate source structure and the interplanetary medium is at best crude compared with examination of the spectrum itself. Therefore, it is important to be able to fit model spectra to the data quickly and accurately. This is what the expansions developed in this dissertation allow.

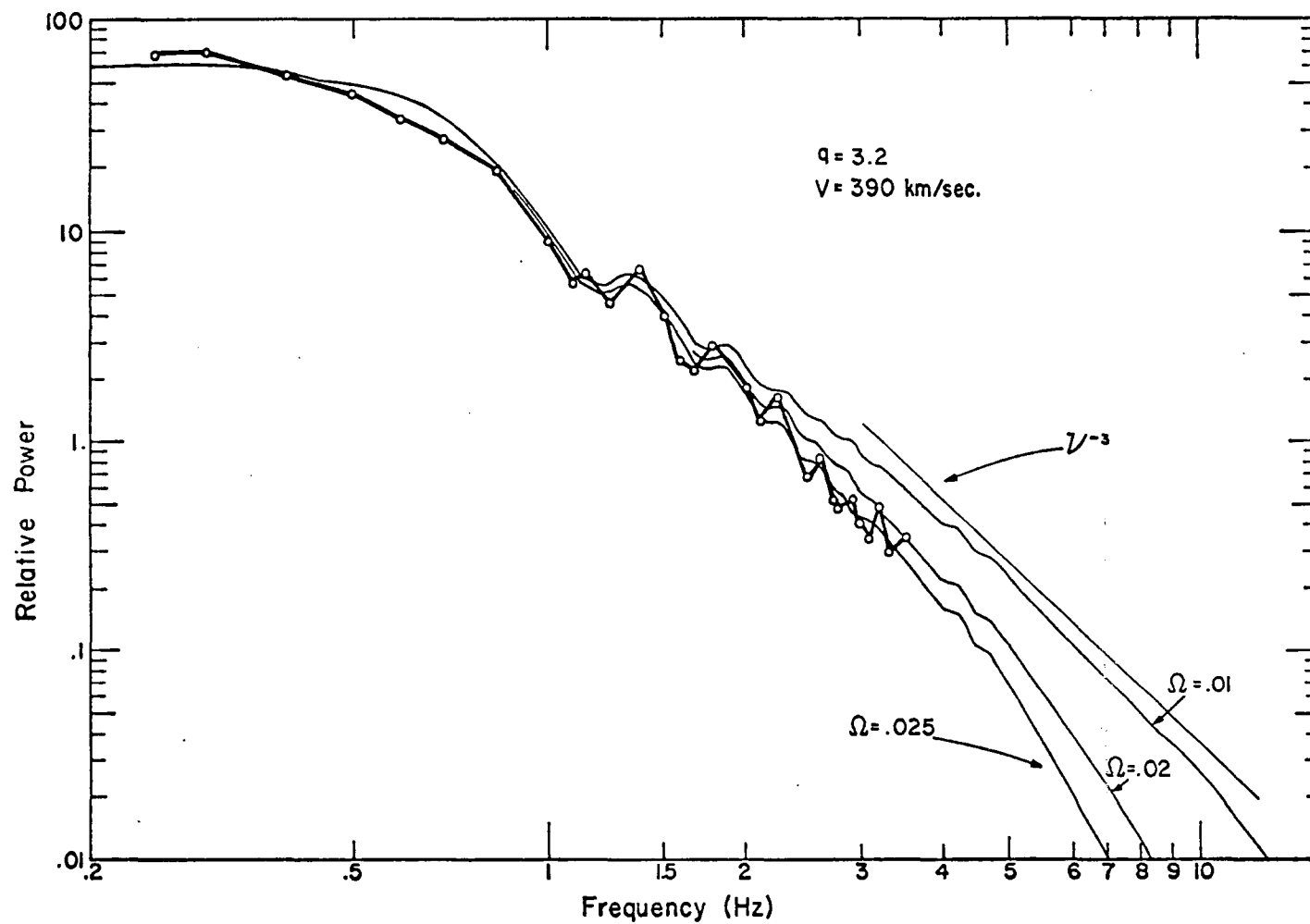


FIGURE 9a

Fit to spectrum published by Lovelace et al., 1970. A quiet medium is assumed, and several source sizes are shown. Power Law index (q) equals 3.6.

$V = 390 \text{ km/sec}$

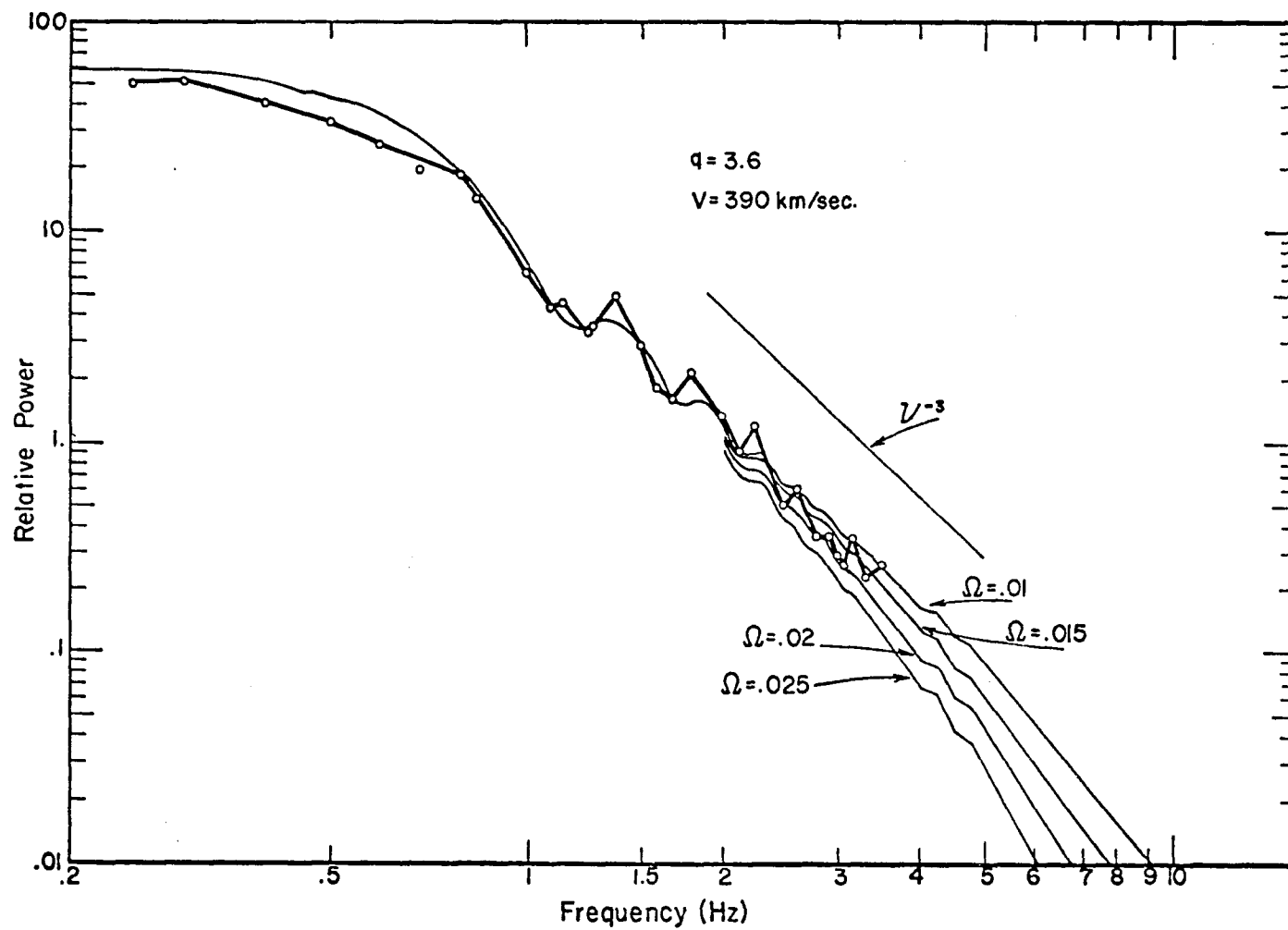


FIGURE 9b

Same as 9a, but with q equal to 3.2, and with different source sizes.

In Figures 9a and 9b, fits to a spectrum published by Lovelace et al. (1970) are given. The parameters are all quite plausible, and the interpretation is that the medium is quiet, with its geometry well modeled by δN_e proportional to ρ^{-4} . The velocity of the solar wind is fit to 390 km/sec. It should be noted that the fit is not absolute in power density (it is absolute in frequencies), but rather a sliding fit. The absolute power is not measured experimentally, nor is it calculated theoretically due to lack of knowledge of the magnitude of either δN_e or k_0 . Only the shape is fit, but this is all that is necessary for a determination of source size, pattern velocity, distance to the scattering medium, and the power law slope. The Lovelace spectrum is fit with two different sets of parameters: either a power law index of 3.6 and a .015 arc-second source, or an index of 3.2 and a source of .025 arc-seconds. More observations would be needed to determine which fit is better. Also fit (Figures 10a and 10b) are two spectra taken from the Cocoa-Cross antenna both on the same day (September 22, 1975). These appear to come from a region closer to earth than would be expected for a quiet medium. They were preceded by enhanced k_p index and as they are to the west of earth, the disturbance associated with the rise in k_p would have co-rotated into the line of sight. Thus it might reasonably be expected that the scattering would be more localized, and be accompanied by high solar wind speeds. A solar wind speed of 600 km/sec was used in the fits, and L values then chosen to bring the

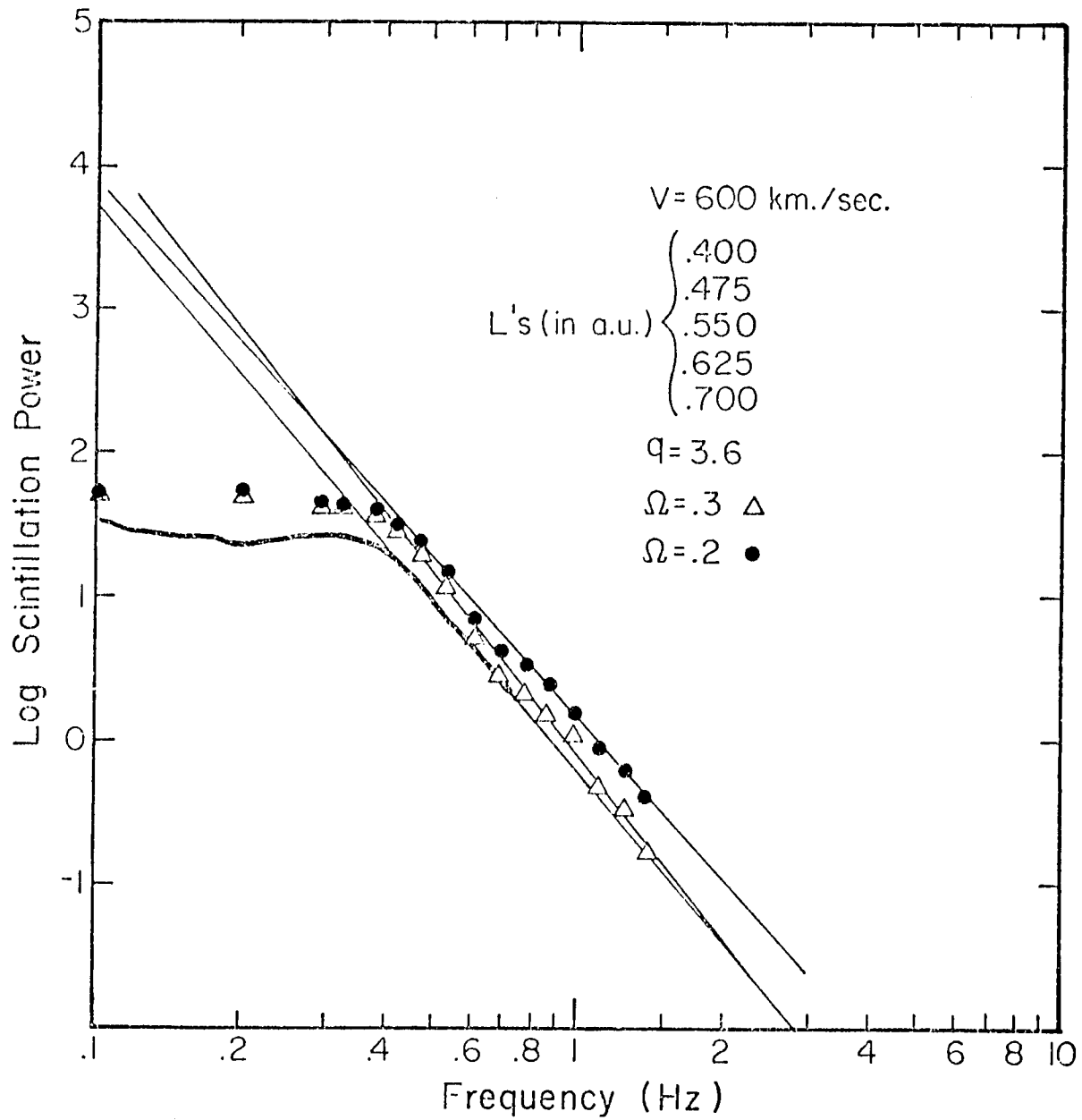


FIGURE 10a

Fit to spectrum of radio source 3C216 taken with COCOA-CROSS antenna. Proper fit lies between the two source sizes used. Note that the computed spectra are off set vertically for clarity. The data were corrected for noise background.

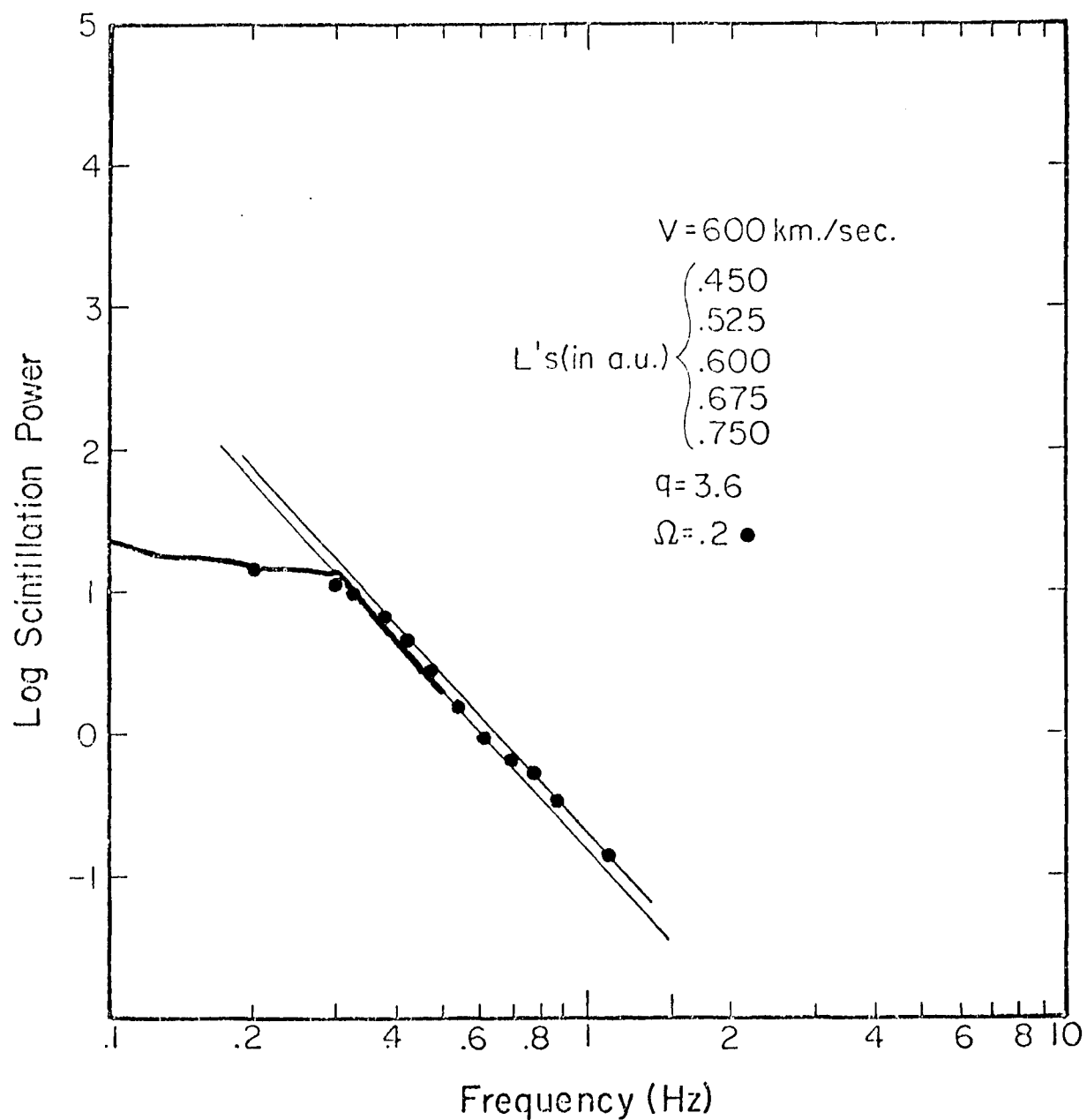


FIGURE 10c

Fit to spectrum of 3C144 taken with COCOA-CROSS antenna. Same day as the spectrum of 10a; the same velocity and power law slope were fit as in 10a but a slightly smaller source size.

Fresnel turn over to the flattening at the observed frequency. A power law index value of 3.6 produced good agreement in both cases. 3C144 (the crab nebula pulsar) was fit with a .2 arc-second angular size, while 3C216 fell between .2 and .3 arc-seconds. A small remnant of Fresnel ripple is evident in the computed spectra, but is missing from the data. This is due to the finite increments in L used in integrating through the medium, and might also indicate that the scattering came from a more extended region than that used in the model. More familiarity with the technique, plus collaboration with other groups using multiple scintillation instruments to independently calculate the solar wind velocity should remove some of the ambiguities still present.

Let us compare the source parameters arrived at in these spectra with those catalogued (at 81.5 MHz) in a paper by Hewish and Readhead, 1974. For the source 3C144, the angular diameter measured is .2", that in the catalogue is .25". For 3C216, the angular diameter measured is .2" - .3", that in the catalogue is .6". This discrepancy could be due to a source with a large axial ratio, and would show up in observations taken at different times of the year. For GTA 21 (Lovelace's spectrum at 430 MHz), the angular diameter measured is $\sim .02$ ", while that listed in the catalogue is .2". This discrepancy could be due to differences in source structure of the two frequencies, or due to the fact that .2" is the lower limit of the Readhead and Hewish catalogue, being essentially indistinguishable from 0" using their technique.

CHAPTER V

SUMMARY

I would like here to outline this work in terms of my contributions to it. The chapter on theory is work done by others, notably Salpeter, 1967, Cronyn, 1970, and Young, 1971. My work in this chapter involves the analytic re-representation of the integral expression for the power spectrum of the scattered power, and includes the dependence on source visibility. This work is outlined in Appendix B. However, the asymptotic series developed in Appendix B was in large part developed by Dr. Roelof, my thesis advisor. He also worked with me on both Appendix A and the rest of Appendix B.

The chapters on Numerical Technique and Discussion represent the bulk of my contribution. This includes a technique for attaining model spectra, scintillation index, and scale without the need for prohibitively expensive and time consuming computation. This will enable the interpretation of large quantities of data, which is needed to carry out many programs of investigation in radio scintillation. This work also allows for the modeling of band-passed data, which is essential to the interpretation of any data, and was a capability hitherto unavailable, to the author's knowledge. Another aspect of this work is the demonstration of the dependence on the distance from the observer of the scintillation power at various frequencies. In addition, the curves of scattering power versus distance are the first of their

kind presented under the assumption of a power law electron density fluctuation spectrum. The analysis of the experimental spectra presented is also original.

BIBLIOGRAPHY

- Abramowitz, M., and I.A. Stegun, Handbook of Mathematical Functions, National Bureau of Standards, 1964.
- Balsley, B.B. and Ecklund, W.L., IEEE Trans. Ant. Prop., AP-20 513-516, 1972.
- Born, M. and Wolf, E., Principles of Optics (third edition) Pergamon Press (London), 1965.
- Bracewell, R., The Fourier Transform and its Applications, McGraw Hill (New York), 1965.
- Budden, K.G. and Uscinski, B.J., The scintillation of extended radio sources when the receiver has a finite bandwidth, Proc. R. Soc. Lond. A330, 65, 1972.
- Burnell, S.J., Enhancements of Interplanetary Scintillation, Corotating Streams, and Forbush Decreases, Nature, 224 356, 1969.
- Callahan, P.S., Interpretation of columnar content measurements of the solar wind turbulence, Astrophys. J., 187, 185, 1974.
- Cronyn, W.M., The analysis of radio scattering and space probe observations of small scale structure in the interplanetary medium, Astrophys. J., 161, 755, 1970.
- Cronyn, W.M., Density fluctuations in the interplanetary plasma: agreement between space probe and radio scattering observations, Astrophys. J. Lett., 171, L101, 1972.
- Cronyn, W.M., and Mitchell, D.G., Interplanetary electron density power spectrum, EOS, 55, 411, 1974.

- Dennison, P. A., and Wiseman, M., Proc. Ast. Soc. Australia, 1, 142, 1968.
- Erdélyi, A., W. Magnus, F. Oberhettinger, F.G. Tricomi, Tables of integral transforms, McGraw Hill (New York) 1954.
- Harris, D.E., Harvard College Obs. Center for Astrophysics Preprint Series No. 129, submitted to Astron. J., 1974.
- Hollweg, J.V., Angular broadening of radio sources by solar wind turbulence, J. Geophys. Res., 75, 3715, 1970.
- Jackson, J.D. ,Classical Electrodynamics, Wiley (New York), 1962.
- Jokipii, J.R., and J.V. Hollweg, Interplanetary scintillations and the structure of solar wind fluctuations, Astrophys. J., 160, 745, 1970.
- Jokipii, J.R., On the "thin-screen" model of interplanetary scintillations, Astrophys. J., 161, 1147, 1970.
- Lovelace, R.V.E., E.E. Salpeter, L.E. Sharp, and D.E. Harris, Analysis of observations of interplanetary scintillations, Astrophys. J., 159, 1047, 1970.
- Matheson, D.N., and L.T. Little, Radio scintillations due to plasma irregularities with power law spectra--the interplanetary medium, Planet. Space Sci., 19, 1615, 1971.
- Mercier, R.P., Diffraction by a screen causing large random phase fluctuations, Proc. Camb. Phil. Soc, 58, 382, 1962.
- Readhead, A.C.S., Interplanetary scintillation of radio sources at metre wavelengths, 2, Mon. Notic. Roy. Astron. Soc., 155, 185, 1971.

- Readhead, A.C.S., and Hewish, A., Galactic structure and the apparent size of radio sources, Nature, 236, 440, 1972.
- Rickett, B.J., Power spectrum of density irregularities in the solar wind plasma, J. Geophys. Res., 78, 1543, 1973.
- Rufenach, C.L., Power-law wave number spectrum deduced from ionospheric scintillation observations, J. Geophys. Res. 77, 4761, 1972.
- Salpeter, E.E., Interplanetary Scintillations I. Theory, Astrophys. J., 147, 433, 1967.
- Sharp, L.E., and Harris, D.E., Enhanced Interplanetary Scintillations associated with Solar Flares, Nature, 213, 377, 1967.
- Tatarskii, V.I., The Effects of the Turbulent Atmosphere on Wave Propagation, (Israel Program for Scientific Translation), U.S. Dept. of Commerce; U.S. National Technical Information Center, 272-277, 1971.
- Unti, T.W.J., Neugebauer, M., and Goldstein, B.E., Direct Measurements of Solar Wind Fluctuations Between .0048 and 13.3 Hz, Astrophys. J., 180, 591, 1973.
- Ward, B.D., Compilation of Solar Particle and Interplanetary Measurements Acquired During the Campaign for Integrated Observations of Solar Flares (CINOF), ed. M.A. Shea and D.F. Smart, Air Force Cambridge Res. Lab, AFCRL-TR-740271, 43-47, 1974.
- Wiseman, M. and Dennison, P.A. Flare Induced Shocks and Corotating Streams in the Interplanetary Medium, Proc. Ast. Soc. Australia, 2, 79, 1972.

Young, A.T., Interpretation of interplanetary scintillations,
Astrophys. J., 168, 543, 1971.

Readhead, A.C.S. and Hewish, A., Fine Structure in Radio Sources
at 81.5 MHz - III. The Survey, Mem. R. Astron. Soc., 78,
1, 1974.

APPENDIX A

Using the form $F(k) = F_0 (k_0^2 + k^2)^{-q/2} \exp(-k^2/2k_i^2)$ for the electron density irregularity power spectrum, where $\alpha \equiv k_0^2/2k_i^2 \ll 1$ since k_0 (the outer scale wave number cut off) is much less than k_i (the inner scale cut off), we obtain an expression for the 3-dimensional electron density irregularity auto-correlation function $A_3(r, k_0, \alpha, q)$.

(A.1)

$$A_3(r, k_0, \alpha, q) = 4\pi F_0 \int_0^\infty dk k^2 (k_0^2 + k^2)^{-q/2} e^{-\alpha(k/k_0)^2} \frac{\sin kr}{kr}$$

Then

(A.2)

$$A_3(0, k_0, \alpha, q) = 4\pi F_0 \int_0^\infty dk k^2 (k_0^2 + k^2)^{-q/2} e^{-\alpha(k/k_0)^2}$$

Letting $t = (k/k_0)^2$

(A.3)

$$A_3(0, k_0, \alpha, q) = 2\pi F_0 k_0^{3-q} \int_0^\infty dt (1+t)^{-q/2} e^{-\alpha t} t^{1/2}$$

Now using an integral relation from Abramowitz and Stegun (1964),

(A.4)

$$\Gamma(a) U(a, b, z) = \int_0^\infty dt e^{-zt} t^{a-1} (1+t)^{b-a-1}$$

where $U(a, b, z)$ is a confluent hypergeometric function, we have

(A.5)

$$A_3(0, k_0, \alpha, q) = 2\pi k_0^{3-q} F_0 \Gamma(\frac{3}{2}) U(\frac{3}{2}, \frac{5}{2}, \alpha)$$

As $k_0^2/2k_1^2 \equiv \alpha \ll 1$, the constant F_0 can be approximated by expanding U for small argument using

$$(A.6) \quad U(a, b, z) = \frac{\pi}{\sin \pi b} \left\{ \frac{M(a, b, z)}{\Gamma(1+a-b)\Gamma(b)} - z^{1-b} \frac{M(1+a-b, z-b, z)}{\Gamma(a)\Gamma(2-b)} \right\}, \quad b \neq 1, 2, 3, \dots$$

$$(A.7) \quad U(a, n+1, z) = \frac{(-)^{n+1}}{n! \Gamma(a-n)} \left[M(a, n+1, z) \ln z + \sum_{r=0}^{\infty} \frac{(a)_r z^r}{(n+1)_r r!} \left\{ \psi(a+r) - \psi(1+r) - \psi(1+n+r) \right\} \right] + \frac{(n-1)!}{\Gamma(a)} z^{-n} M(a-n, 1-n, z)_n$$

$n = 0, 1, 2, \dots$

$$(A.8) \quad M(a, b, z) = 1 + \frac{a}{b} z + \frac{(a)_2 z^2}{(b)_2 2!} + \dots + \frac{(a)_n z^n}{(b)_n n!} + \dots$$

$$(A.9) \quad (a)_n = a(a+1)(a+2) \dots (a+n-2)(a+n-1)$$

where $\psi(a) = \Gamma'(a)/\Gamma(a)$ and $(a)_0 = 1$. $M(a-n, 1-n, z)_n$ signifies the series above for M, to n terms. However, as α is much less than unity, we can go back to equation A-1 more simply. For $\alpha = 0$

$$(A.10) \quad A_3(r, k, 0, q) = \frac{4\pi F_0}{r} \int_0^\infty dk k (k^2 + k^2)^{-\frac{1}{2}} \sin kr$$

Using

$$(A.11) \quad \int_0^\infty dx x (x^2 + a^2)^{\nu - \frac{3}{2}} \sin xy = \begin{cases} \frac{\sqrt{\pi} (2a)^\nu y^{1-\nu}}{\Gamma(\frac{3}{2} - \nu)} K_\nu(ay) \\ \frac{\pi y e^{-ay} a^{(3-2n)}}{2^{2n-1} (n-1)!} \sum_{m=0}^{n-2} \frac{(2n-m-4)!}{m! (n-m-2)!} \\ \quad (\nu = (\frac{3}{2} - n), n=2,3,4,\dots) \end{cases}$$

$\operatorname{Re} a > 0$
 $\operatorname{Re} \nu < 1$

from Erdélyi, et al.--Tables of Integral Transforms (1954),

we then have

$$(A.12) \quad A_3(\alpha=0) = \frac{F_0 2\pi^{\frac{3}{2}}}{\Gamma(\frac{q}{2})} \left(\frac{r}{2k_0}\right)^{\frac{q-3}{2}} K_{\frac{3-q}{2}}(k_0 r)$$

and

$$(A.13) \quad A_3(\alpha=0, q=4) = \frac{F_0 \pi^2}{k_0} e^{-k_0 r}$$

Note that for $q > 3$

(A.14)

$$A_3(0, k_0, 0, q) = \frac{F_0 \pi^{\frac{3}{2}}}{\Gamma(\frac{q}{2})} \Gamma(\frac{q-3}{2}) k_0^{3-q} = \langle (\Delta N_c)^2 \rangle$$

Thus defining F_0 .

APPENDIX B

$$(B.1) \quad dP = \frac{dL}{V_1} (2\pi r_e \lambda)^2 F_0 \int_{-\infty}^{\infty} dk_y (\gamma k_x^2 + k_y^2)^{-\frac{1}{2}} \sin^2\left(\frac{k_x^2 + k_y^2}{k_f^2}\right) e^{-\frac{\beta k_x^2 + k_y^2}{2 k_f^2}}$$

Defining

$$(B.2) \quad dP \equiv \frac{dL}{V_1} (2\pi r_e \lambda)^2 F_0 \Gamma(\frac{1}{2}) k_f^{1-\beta} J(s, \gamma, s_1, \beta, \beta)$$

$$(B.3) \quad J = \frac{1}{\Gamma(\frac{1}{2})} \int_0^{\infty} dt (\gamma s + t^2)^{-\frac{1}{2}} \sin^2(s + t^2) e^{-\frac{\beta s}{2 s_1}} e^{-\frac{t^2}{2 s_1}}$$

where $s = k_x^2/k_f^2$, $s_1 = k_1^2/k_f^2$, and $t = k_y/k_f$

$$(B.4) \quad J = \frac{1}{2 \Gamma(\frac{1}{2})} \int_0^{\infty} dt (\gamma s + t^2)^{-\frac{1}{2}} (1 - \cos 2(s + t^2)) e^{-\frac{\beta s}{2 s_1}} e^{-\frac{t^2}{2 s_1}}$$

$$(B.5) \quad = \frac{e^{-\frac{\beta s}{2 s_1}}}{2 \Gamma(\frac{1}{2})} \left[\int_0^{\infty} dt (\gamma s + t^2)^{-\frac{1}{2}} e^{-\frac{t^2}{2 s_1}} - \operatorname{Re} \left\{ \int_0^{\infty} dt (\gamma s + t^2)^{-\frac{1}{2}} e^{-\frac{t^2}{2 s_1} + 2i t^2 + 2i s} \right\} \right]$$

Letting $\gamma s \xi = t^2$

$$(B.6) \quad J = \frac{1}{\Gamma(\frac{1}{2})} (\gamma s)^{\frac{1-\beta}{2}} e^{-\frac{\beta s}{2 s_1}} \left[\int_0^{\infty} d\xi \xi^{-\frac{1}{2}} e^{-\frac{\gamma s \xi}{2 s_1}} (1 + \xi)^{-\frac{1}{2}} \right. \\ \left. - \operatorname{Re} \left\{ e^{i 2 s} \int_0^{\infty} d\xi \xi^{-\frac{1}{2}} (1 + \xi)^{-\frac{1}{2}} e^{-\gamma s \xi \left(\frac{1}{2 s_1} - 2i \right)} \right\} \right]$$

which yields, using relation (A4) in Appendix A

$$(B.7) \quad J = e^{-\frac{\theta S}{2S_1}} (\gamma S)^{\frac{1-\ell}{2}} \operatorname{Re} \left\{ U\left(\frac{1}{2}, \frac{3-\ell}{2}, \frac{\gamma S}{2S_1}\right) - e^{i2S} U\left(\frac{1}{2}, \frac{3-\ell}{2}, \gamma S \left[\frac{1}{2S}, -2i\right]\right) \right\}$$

From Abramowitz and Stegun (1964) the expansion of $U(a, b, z)$ for $|z| \gg 1$ is

$$(B.8) \quad U(a, b, z) \sim z^{-a} \left\{ \sum_{n=0}^{R-1} \frac{(a)_n (1+a-b)_n}{n!} (-z)^{-n} + O(|z|^{-R}) \right\} \\ \left(-\frac{3}{2}\pi < \arg z < \frac{3}{2}\pi \right)$$

However, this expansion proved to converge too slowly to meet the requirements of this application. Therefore, the following presents a derivation of an expansion which was subsequently used in the expansions for J .

Rewriting relation (A4), we have

$$(B.9) \quad \Gamma(a) U(a, b, z) = \int_0^\infty dt e^{-zt} t^{a-1} [e^t + (t+1-e^t)]^{b-a-1}$$

now

$$(B.10) \quad [e^t + (t+1-e^t)]^{b-a-1} = \sum_n \binom{b-a-1}{n} (t+1-e^t)^n e^{t(b-a-1-n)}$$

where

$$(B.11) \quad \binom{b-a-1}{n} = \frac{\Gamma(b-a)}{\Gamma(n+1)\Gamma(b-a-n)}$$

so

$$(B.12) \quad \Gamma(a) \mathcal{U}(a, b, z) = \sum_n \frac{\Gamma(b-a)}{n! \Gamma(b-a-n)} \int_0^\infty dt e^{-(z+a+1-b+n)t} t^{a-1} (t+1-e^t)^n$$

but

$$(B.13) \quad (t+1-e^t)^n = (-1)^n \left(\frac{t^2}{2!} + \frac{t^3}{3!} + \dots \right)^n \equiv \frac{t^{2n}}{(-2)^n} \sum_{m=0}^{\infty} K_{nm} t^m$$

so

$$(B.14) \quad \Gamma(a) \mathcal{U}(a, b, z) = \sum_n \sum_m \frac{\Gamma(b-a) K_{nm}}{(-2)^n n! \Gamma(b-a-n)} \int_0^\infty dt e^{-(z+a+1+n-b)t} t^{a-1+2n+m}$$

$$(B.15) \quad = \sum_n \sum_m \frac{\Gamma(b-a) K_{nm}}{(-2)^n n! \Gamma(b-a-n)} \Gamma(a+2n+m) (z+a+1+n-b)^{-(a+2n+m)}$$

$$(B.16) \quad \mathcal{U}(a, b, z) = \sum_n \sum_m \frac{K_{nm}}{(-2)^n n!} (b-a-n)_n (a)_{2n+m} (z+a+1+n-b)^{-(a+2n+m)}$$

where

$$(B.17) \quad K_{0m} = \delta_{0m}, \quad K_{1m} = \frac{2}{(m+2)!}, \quad K_{n+1,m} = \sum_{l=0}^m \frac{2 K_{nl}}{(2+m-l)!}$$

and

$$(B.18) \quad (a)_n = a(a+1)(a+2)\dots(a+n-2)(a+n-1) = \frac{\Gamma(a+n)}{\Gamma(a)}$$

Then, to the first few terms,

$$(B.19) \quad \begin{aligned} \mathcal{U}(a, b, z) \sim & (z+a+1-b)^{-a} - \frac{1}{2} (b-a-1)(a+1)a (z+a+2-b)^{-(a+2)} \\ & - \frac{1}{6} (b-a-1)(a+2)(a+1)a (z+a+2-b)^{-(a+3)} \\ & - \frac{1}{24} (b-a-1)(a+3)(a+2)(a+1)a (z+a+2-b)^{-(a+4)} \\ & + \frac{1}{8} (b-a-2)(b-a-1)(a+3)(a+2)(a+1)a (z+a+3-b)^{-(a+4)} \end{aligned}$$

Now using

$$(B.20) \quad z = \xi - i\eta, \quad (z + a + 1 + n - b) = \omega_n e^{-i\theta_n}$$

where

$$(B.21) \quad \omega_n^2 = \eta^2 + (\xi + a + 1 + n - b)^2, \quad \theta_n = \tan^{-1} \frac{\eta}{(\xi + a + 1 + n - b)}$$

for $a = .5$ (our case)

$$(B.22) \quad \begin{aligned} U\left(\frac{1}{2}, b, z\right) \simeq & \omega_1^{-\frac{1}{2}} e^{i\frac{\theta_0}{2}} - (b-1.5) .375 \omega_1^{-2.5} e^{i(2.5\theta_1)} \\ & - .3175 (b-1.5) \omega_1^{-3.5} e^{i(3.5\theta_1)} \\ & - .2734375 (b-1.5) \omega_1^{-4.5} e^{i(4.5\theta_1)} \\ & + .8203125 (b-2.5)(b-1.5) \omega_2^{-4.5} e^{i(4.5\theta_2)} \end{aligned}$$

This series converges very rapidly for $|z| \geq 1$; $e^{i2s} U(\frac{1}{2}, b, z)$ is the same expansion, with $i2s$ added to the exponent of each of the exponentials.

U. of Iowa 75-1

APPENDIX C

Interplanetary Scintillation Observations
with the Cocoa Cross Radio Telescope*

by

W. M. Cronyn, S. D. Shawhan,
F. T. Erskine, A. H. Huneke,
and
D. G. Mitchell

W. M. Cronyn
Space Environment Laboratory/ERL
National Oceanic and Atmospheric Administration
Boulder, Colorado 80302

S. D. Shawhan, F. T. Erskine, A. H. Huneke
Department of Physics and Astronomy
University of Iowa
Iowa City, Iowa 52242

D. G. Mitchell
Department of Physics
University of New Hampshire
Durham, New Hampshire 03824

February, 1975

Submitted as a Letter to Nature-Physical Sciences.

*Located at the University of Maryland Clark Lake Radio Observatory,
Borrego Springs, CA 92004. Research supported by NSF Grant (Atmos.
Science Section) DES73-06559A01, NASA Purchase Request S-57016A,
NASA Grant NGL16-001-002 and NOAA Contract 04-3-022-28.

INTERPLANETARY SCINTILLATION OBSERVATIONS WITH THE COCOA CROSS RADIO TELESCOPE

We report the first IPS (interplanetary scintillation) observations made with the 34.3 MHz (Cocoa Cross radio telescope, a joint project of the National Oceanic and Atmospheric Administration and the University of Iowa. The instrument has one of the largest effective collecting areas of any radio telescope in the world, more than $7 \times 10^4 \text{ m}^2$ (approximately equal to the geometric area of the 300 m Arecibo reflector). It has been specifically designed for synoptic IPS observations of large numbers of radio sources at source-sun elongation angles of 20° to 180° covering southern ecliptic latitudes of 0° to 45° (depending on ecliptic longitude) and the entire northern ecliptic hemisphere. Observing this grid of sources daily we intend to locate, map and track co-rotating and transient solar wind features such as streams, blast waves and plasmoids as identified by associated IPS activity¹⁻⁵. These observations are being correlated with measurements of interplanetary magnetic fields, solar wind velocity, electron number density and energetic particles as well as H_α maps and geomagnetic activity.

Technical parameters of the Cocoa Cross radio telescope are given in Table 1. A simplified block diagram of the receiver electronics is presented in Figure C 1. To obtain the main beam response the North and South arm signals are amplified, filtered and summed at 34.3 MHz, down-converted to

20 MHz, amplified under strong automatic gain control and correlated against the East-West arm signals using a double-balanced mixer. Other correlation products are also measured to provide beam pointing and array performance information. The resultant normalized main beam correlation product is then smoothed to give the total power of the source, I , and is also bandpass filtered in the range 0.1 to 1.5 Hz giving the fluctuation power, F , and squared (self-multiplied) and smoothed to give the scintillation power, S ; the 0.1-1.5 Hz signal is also differentiated, squared and smoothed to give the "differentiated power", D . The scintillation index is then estimated as $m = k_m \sqrt{S/I}$, and the frequency scale of the scintillations (square-root second moment of the power spectrum) is $f = k_f \sqrt{D/S}$, where k_m and k_f are gain constants. These and other receiver outputs are presently displayed on a multichannel paper chart recorder (see Figure 2). All necessary telescope and receiver functions such as beam steering, calibration and gain changes are card reader controlled allowing unattended operation. (Further details are given in a NOAA/SEC technical report in publication.)

The three characteristics of the telescope which make it particularly well suited for the measurement of IPS index and frequency scale for large numbers of sources are:

- (1) large collecting area, (2) relatively high angular resolution, and (3) large spatial extent. Feature (1) is necessary for measurements of IPS parameters of weak sources (≈ 10 f.u.); (2) is necessary to avoid serious confusion problems and to make possible the determination of normalized IPS index for

every source without consideration of array response variation, ionospheric effects or source intensity variability. With regard to feature (3), ionospheric scintillation frequencies < 0.1 Hz are eliminated by the bandpass filter while frequency components above 0.1 Hz are severely attenuated by aperture filtering⁷. The spatial extent, L , of ionospheric frequency components greater than frequency ν_c can be estimated from the relationship

$$(C.1) \quad L \approx U/2\pi\nu_c$$

where U is the diffraction pattern speed. For $\nu_c = 0.1$ Hz and using $U < 0.15$ km/sec (appropriate for ionospheric wind speeds), $L \approx .25$ km which is less than the 1 km spatial extent of the array, resulting in averaging over several independent scintillation patches. By contrast, for solar wind velocities of 400 km/sec and $\nu_c = 1.5$ Hz, the spatial extent of components for $\nu < \nu_c$ is $L \approx 40$ km $\gg 1$ km. Beyond 1.5 Hz there is no significant IPS energy for most sources at 34 MHz. Typical data records are shown in Figure C 2 Source solar ecliptic coordinates range in longitude between 22°W and 12°E, in latitude from 19°N to 59°N, and in elongation angle from 32° to 60°. The increase in raw fluctuation signal F can be seen clearly for 3C280 and 3C295. Measurable scintillation indices are 0.1(3C293) to 0.2 (3C286); frequency scales are 0.4 Hz (3C280) to 0.6 Hz (3C295). In Figure C 3 we show observations of a source taken on four successive days at solar ecliptic longitude 128°E, latitude 16°, elongation angle of 126°. Scintillation index is 0.11 for days 328 and 329; 0.07 for 330 and 331.

It is illustrative of both daily index variability and IPS at large elongation angles.

The effectiveness of the ionospheric scintillation suppression has been confirmed by numerous observations of large angular diameter sources such as 3C405. These sources display strong ionospheric scintillations but not within the frequency range of 0.1 to 1.5 Hz on the Cocoa-Cross telescope (except during extraordinary ionospheric activity).

Interpretation of the observations to date have revealed recurrent scintillation activity displaying a 27 day periodicity over a seven month period as well as a scintillation event on 26 June which was probably associated with a blast wave, a geomagnetic storm sudden commencement, and a solar particle event (papers presented at Fall 1974 URSI and AGU meetings and in preparation for J. Geophys. Res.).

From our initial IPS observations at 34.3 MHz we make the following general conclusions: (1) even though IPS-quenching interstellar scattering effects are more pronounced at our observing frequency⁸⁻¹⁰, we have observed more than 65 scintillating sources (some at less than 15° galactic latitude) out of approximately 100 sources, implying a larger number of decametric wavelength sources with second-of-arc structure; (2) IPS activity is highly variable even at large solar elongation angles; (3) IPS activity is sometimes observed at high ecliptic latitudes which has no apparent correlation with low latitude activity; (4) IPS can be observed on some sources to within less than 20° of the sun; (5) ionospheric scintillation effects can be suppressed by a combination of bandpass and

aperture filtering.

In addition to the IPS studies, observational programs dealing with planetary sources, pulsars, flare stars and x-ray sources are underway.

We acknowledge the encouragement of Dr. Norman F. Ness, Dr. Donald J. Williams, and Prof. James A. Van Allen and the support of NASA, NOAA, and the Atmospheric Science Section of NSF.




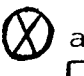


TABLE 1

PARAMETERS OF THE COCOA-CROSS RADIO TELESCOPE

A. Array Type:	Mills Cross	135.5^λ EW x 95.25^λ NS
B. Linear Dimensions	NS Arm	66m EW x 832m NS
	EW Arm	1184m EW x 46m NS
C. Antenna Elements:	Type	Balsley-Ecklund ⁶ Colinear-Coaxial
	Polarization	East-West
	Length	NS Arm 7.2^λ EW Arm 3.8^λ
	EW Beamwidth	NS Arm 8° EW Arm 15°
D. Element Organization:	NS Arm	128 elements spaced 0.75^λ NS
	EW Arm	256 elements in 32 banks spaced 4^λ EW with 8 elements per bank spaced 0.75^λ NS
E. Feed and Phasing:	Branch feed, diode-switch-controlled tapped phasing lines with real-time delay control for wideband coherence.	
F. Steering:	NS	$\pm 60^\circ$ from zenith, $33^\circ \pm 60^\circ$ in declination.
	EW	meridian transit ± 10 minutes
G. Beamwidth	NS Arm	8° EW x 0.6° secant (z) NS
	EW Arm	0.4° EW x 11° NS
	Composite	0.4° EW x 0.6° secant (z) NS
H. Collecting Area:	NS Arm	$3.5 \times 10^4 \text{ m}^2$
	EW Arm	$3.7 \times 10^4 \text{ m}^2$
	Total	$7.2 \times 10^4 \text{ m}^2$
I. Array Response:	$26^\circ\text{K}/10^{-26}\text{W/m}^2\text{-Hz}$ (uniform illumination)	
J. Center Frequency:	34.3 MHz	($\lambda = 8.75$ meters)
K. Bandwidth	1 MHz maximum	

FIGURE CAPTIONS

Figure C1 Simplified block diagram of RF, IF and post detection

circuitry. Symbols:  amplifier;  iso-T;
 double balanced mixer;  analog multiplier;
 30 second RC time constant;  RC differentiator.

L.O. frequency is 54.3 MHz, IF is 20 MHz. Not shown are additional amplifiers and filters, and circuitry for measuring additional correlation products.

Figure C2 Observations taken on 5 October 1974. Data channels are identified as in Figure 1. Relative sensitivity of channels is constant in time except on channel S which is reduced by 4 during transit of 3C280. Polarity of correlation response I can be either positive or negative. Channel F is the raw fluctuation power; channels D, S and I_{30} have a 30 second time constant and are therefore delayed by 30 seconds with respect to channel I_1 which has a 1 second time constant. Rectangular spikes on I_1 are calibration signals after rephasing for the next source.

Figure C3 Observations of Quasar 3C186 taken between 24 and 27 November 1974. Channels are identified as in Figure 2. Rectangular pulse after transit on channel I_1 is rephasing and calibration. Scintillation activity changes significantly between days 329 and 330.

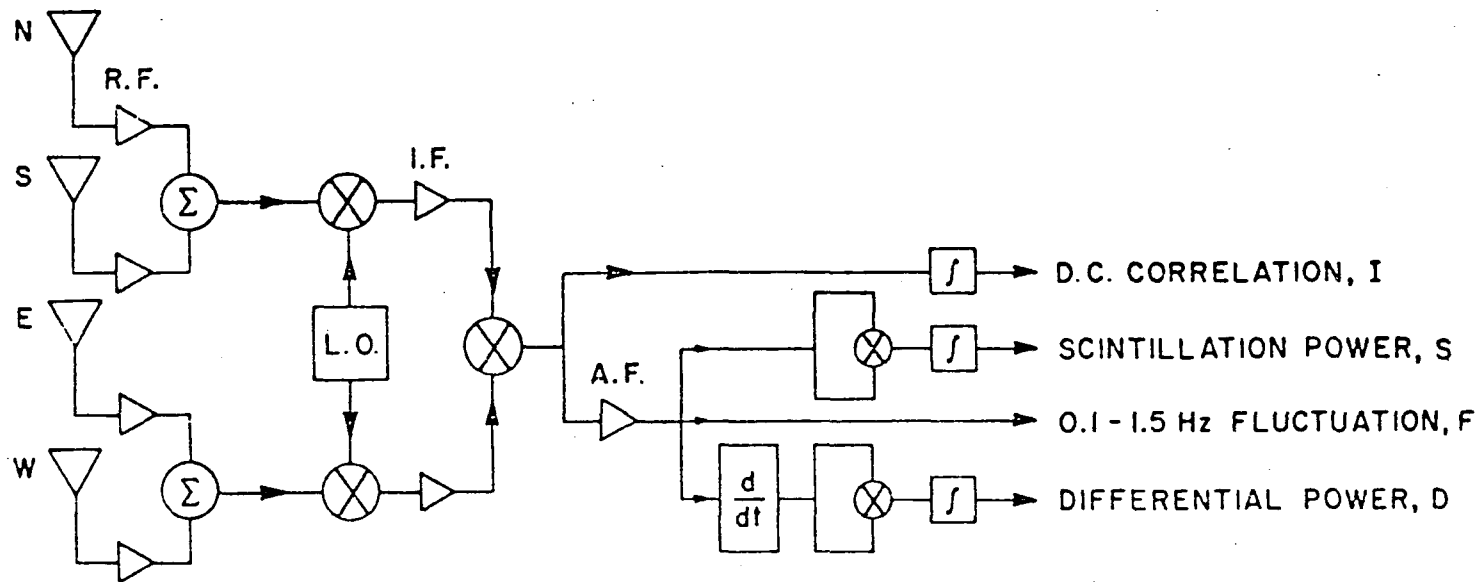


FIGURE C 1

Block Diagram of COCOA CROSS Radio Telescope

A-675-59

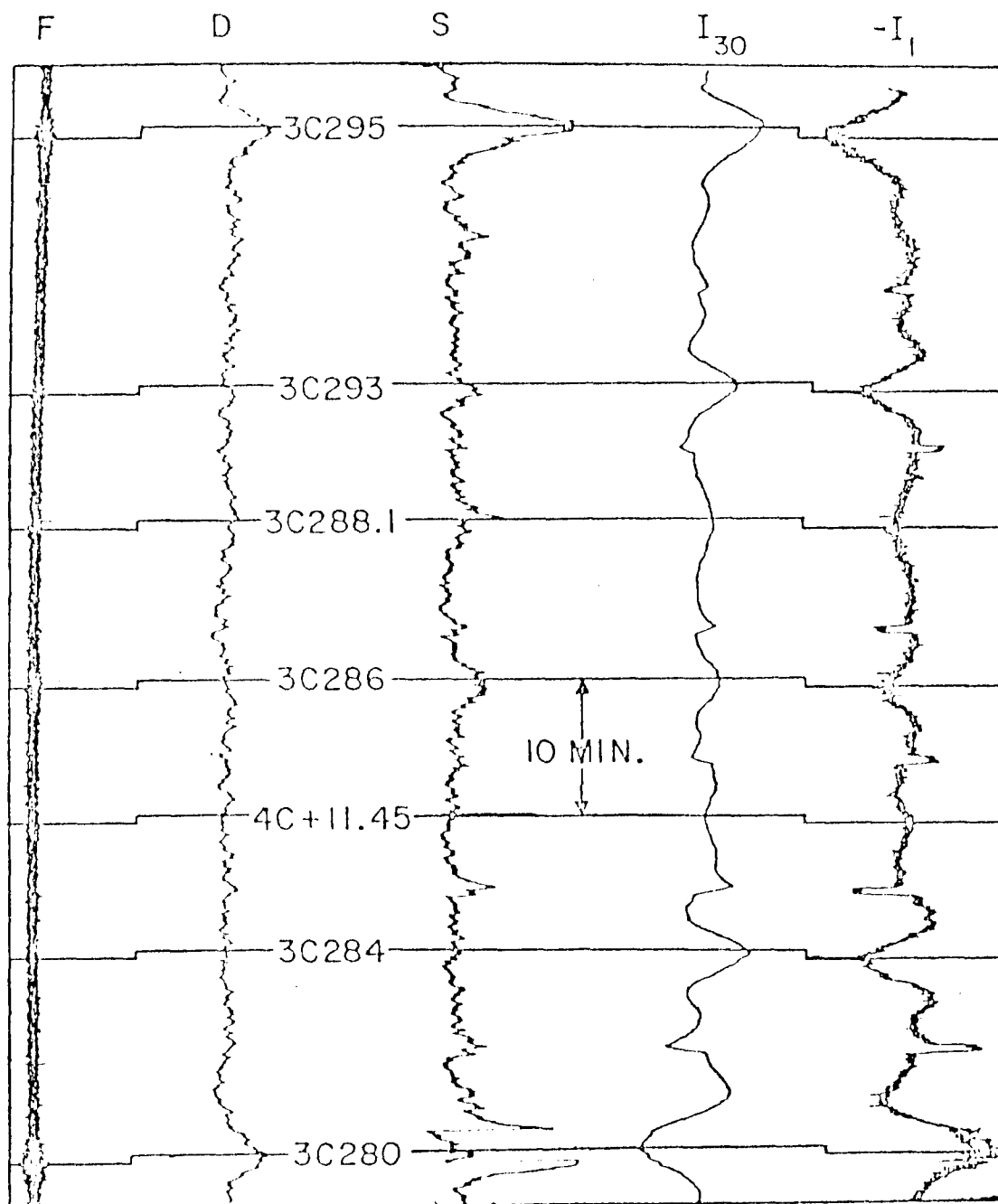


FIGURE C 2

Observations on COCOA CROSS Telescope October 5, 1974.

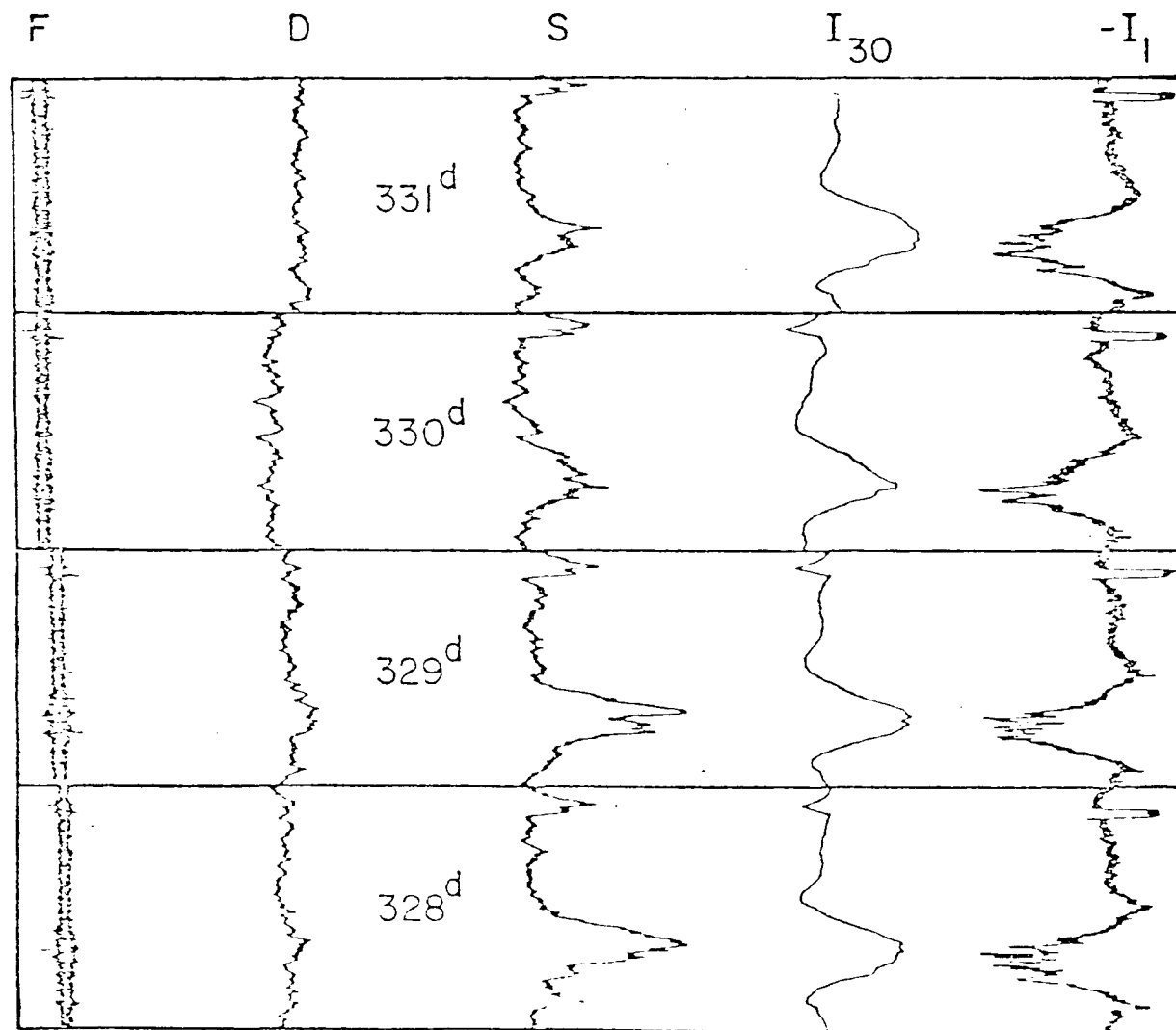


FIGURE C 3

Observations on COCOA CROSS Telescope between November 24 and November 27, 1974.